Clim Dyn (2009) 32:525–548
DOI 10.1007/s00382-008-0421-7

The Southern Westerlies during the last glacial maximum in PMIP2 simulations

Maisa Rojas · Patricio Moreno · Masa Kageyama · Michel Crucifix · Chris Hewitt · Ayako Abe-Ouchi · Rumi Ohgaito · Esther C. Brady · Pandora Hope

Received: 3 October 2007 / Accepted: 7 May 2008 / Published online: 3 June 2008

Abstract The Southern Hemisphere westerly winds are an important component of the climate system at hemispheric and global scales. Variations in their intensity and latitudinal position through an ice-age cycle have been proposed as important drivers of global climate change due to their influence on deep-ocean circulation and changes in atmospheric CO_2. The position, intensity, and associated climatology of the southern westerlies during the last glacial maximum (LGM), however, is still poorly understood from empirical and modelling standpoints. Here we analyse the behaviour of the southern westerlies during the LGM using four coupled ocean-atmosphere simulations carried out by the Palaeoclimate Modelling Intercomparison Project Phase 2 (PMIP2). We analysed the atmospheric circulation by direct inspection of the winds and by using a cyclone tracking software to indicate storm tracks. The models suggest that changes were most significant during winter and over the Pacific ocean. For this season and region, three out four models indicate decreased wind intensities at the near surface as well as in the upper troposphere. Although the LGM atmosphere is colder and the equator to pole surface temperature gradient generally increases, the tropospheric temperature gradients actually decrease, explaining the weaker circulation. We evaluated the atmospheric influence on the Southern Ocean by examining the effect of wind stress on the Ekman pumping. Again, three of the models indicate decreased upwelling in a latitudinal band over the Southern Ocean. All models indicate a drier LGM than at present with a clear decrease in precipitation south of 40°S over the oceans. We identify

M. Rojas (✉)
Department of Geophysics,
University of Chile Blanco Encalada,
2002 Santiago, Chile
e-mail: maisa@dgf.uchile.cl

M. Rojas · P. Moreno
Institute of Ecology and Biodiversity, Santiago, Chile

P. Moreno
Department of Ecological Sciences, University of Chile,
Las Palmeras, 3425 Santiago, Chile

M. Kageyama
LSCE/IPSL, UMR CEA-CNRS-UVSQ 1572, CE Saclay,
L'Orme des Merisiers Bat. 701, 91191 Gif-sur-Yvette Cedex,
France

M. Crucifix
Institut d'Astronomie et de Géophysique G. Lemaitre,
Université catholique de Louvain, Chemin du Cyclotron,
2, 1348 Louvain-la-Neuve, Belgium

C. Hewitt
Met Office, FitzRoy Road, Exeter, Devon EX1 3PB, UK

A. Abe-Ouchi
Center for Climate System Research,
The University of Tokyo, 5-1-5 Kashiwanoha,
Kashiwa 277-8568, Japan

R. Ohgaito
Frontier Research Center for Global Change,
Japan Agency for Marine-Earth Science and Technology,
Showa-machi 3173-25, Kanazawa-ward, Yokohama,
Kanagawa 236-0001, Japan

E. C. Brady
Climate Change Research National Center for Atmospheric
Research, 1850 Table Mesa Drive, P.O. Box 3000, Boulder,
CO 80307, USA

P. Hope
Bureau of Meteorology Research Centre, GPO Box 1289,
Melbourne, VIC 3001, Australia

important differences in precipitation anomalies over the land masses at regional scale, including a drier climate over New Zealand and wetter over NW Patagonia.

1 Introduction

The behaviour of the southern westerlies and the adjacent Southern Ocean during the last glacial maximum (LGM 21 kyr, Kyr = 1,000 calendar years before present) and the last glacial–interglacial transition (LGIT, ~18–11 kyr) is still poorly understood despite its fundamental role on modern hemispheric and global climate. A conceptual palaeoclimate model by Imbrie et al. (1992) suggested that the wind stress imparted by the westerlies on the Southern ocean at and south of the latitude of Drake Passage (50°–60°S) may greatly influence the global thermohaline circulation during glacial terminations. They proposed that the northward flow of surface waters forced by the stress of the westerly winds help drive deep thermohaline currents into the Antarctic region. Variations in this mechanism through an ice-age cycle would be linked to the intensity and latitudinal position of the southern westerlies (Imbrie et al. 1992). More recently, Toggweiler et al. (2006) developed an idealised general circulation model of the ocean's deep circulation and atmospheric CO_2 fluxes that addresses some key elements of glacial-interglacial transitions. Among those are CO_2 cycles, the tight correlation between atmospheric CO_2 and Antarctic temperatures, the lead of Antarctic temperatures over CO_2 at terminations, and inter-hemispheric alternations in the ocean's $\delta^{13}C$ minimum values. Toggweiler et al. (2006) hypothesised that these transitions occur through a positive feedback that involves the mid-latitude westerly winds in the Southern Hemisphere, the mean temperature of the atmosphere, and the overturning of southern deep water. In this scenario, extreme glacial conditions are coupled with an equatorward shift of the westerlies, allowing more respired CO_2 to accumulate in the deep ocean. The opposite state, warm interglacial climates, would be associated with a poleward shift of the westerlies that would trigger a release of respired CO_2 out of the deep ocean via surface wind stress (Ekman divergence) imparted by the westerlies on the surface of the Southern ocean. Hence, tracking the ice-age history of the southern westerlies is of fundamental importance for understanding the origin and propagation of palaeoclimate signals, the coupling of the ocean–atmosphere in the extra-tropics, and the interaction of low- and high-latitude climate controls on hemispheric and global climate.

The exact timing of variations of the southern westerlies during the LGIT, as well as the magnitude of these variations, are a subject of active discussion (Heusser et al. 1999; Lamy et al. 1998, 1999; Moreno et al. 1999; Valero-Garcés et al. 2005), and there are important differences between and within terrestial and marine archives.

1.1 Palaeoclimate proxies

There are a number of palaeoclimate proxies that directly or indirectly tell us about wind speed and past precipitation regimes. Direct proxy of wind intensity are dust records and oceanic upwelling, whereas pollen records and variations in terrigenous supply to offshore environments could be considered indirect proxies of wind speed. Wind intensity affects precipitation, and in the southern hemisphere extratropics the precipitation is mainly produced in winter by fronts and low-pressure systems embedded in the prevailing westerly circulation (e.g. Garreaud 2007). In addition orographic rainfall is an important component of the total precipitation in New Zealand and the southern Andes. In these regions the existing mountain ranges exert strong east–west dry-wet gradients. Therefore during periods of reduced westerly flow, these east–west contrasts may be reduced.

A recent synthesis of Palaeoclimate records from Australia (Turney et al. 2006) spanning between 30 and 8 kyr, indicates colder conditions (ΔT: 9–11°C), widespread desiccation of lakes, and more intense aeolian activity during the LGM. Likewise, New Zealand records of stalagmites are interpreted as indicative of colder and relatively drier conditions (Williams et al. 2005) during the LGM, contemporaneous with maximum glacial extent in South Island (Schaefer et al. 2006), and stronger-than-present surface wind speeds are deduced from the enhanced deposition of aeolian Quartz (Alloway et al. 1992). A synthesis by Shulmeister et al. (2004) concludes that the LGM was a period of enhanced westerlies between 36° and 43°S over the Australasian sector. That synthesis incorporates a large number of palaeoclimate proxies, including terrestial and marine dust, upwelling, glacial advances, ice cores and vegetation changes. Dust records from southern Australia and New Zealand suggest maximum wind speeds during the LGM, with a modest equatorward deflection of 3°. This is of similar magnitude to modern variability associated to ENSO events. Around the New Zealand region there is widespread evidence for increased upwelling at the LGM. Shulmeister et al. (2004) further reports that pollen records in southern Australia indicate colder and drier conditions compared to present. Pollen records in New Zealand (South Island) indicate grassland and shrubland vegetation east of the southern Alps during the LGM, this type of land cover are most likely linked to frost, drought and high winds.

In South America, the majority of palaeoclimate records north of 42°S in the SE Pacific sector estimate an increase and/or northward shift of the westerly belt relative to modern conditions sometime during the LGIT. Lake cores suggest wetter than present conditions during the LGM (Valero-Garcés et al. 2005). Twice as much precipitation and 6°–7° colder conditions compared to present day are inferred from a pollen records at 41°S by Moreno et al. (1999) and Heusser et al. (1999). Proxy analysis of terrigenous material found in offshore sediment cores from central Chile (27°–33°S) (Lamy et al. 1998, 1999) suggest increased rainfall brought by equatorward-shifted westerlies throughout the LGM.

Latitudinal shifts in the zone of maximum precipitation associated with the southern westerlies in the South American sector have been invoked as a possible cause for the apparent mismatch in the timing and extent of glacial advances during the LGM in different sectors of Patagonia (39°–54°S) (Denton et al. 1999; Douglass et al. 2005; Moreno and Leon 2003; Sugden 2005). Therefore, modelling the geographic and temporal variations of the southern westerlies during the LGM and LGIT are critical for assessing the meaning and implications of paleoclimatic data for reconstructing past climate dynamics at regional and hemispheric scales.

1.2 Previous modelling studies

As described above, a consensus is emerging from the paleoclimatic records for enhanced westerly wind speeds and its effect on the precipitation in the SH midlatitudes, and this evidence has helped to develop various conceptual models for palaeoclimate change during glacial–interglacial transitions (Toggweiler et al. 2006; Williams and Bryan 2006). Yet the climate modelling studies still have not converged into a clear picture of how and why the changes in the westerly circulation occurred.

Most of the earlier modelling studies aimed towards understanding the palaeoclimate evolution in the Southern Hemisphere were carried out under the Paleoclimate Intercomparison Project framework (PMIP1, Joussaume et al. 1999). The experimental design of the PMIP1 simulations, for the LGM climate, included atmospheric global circulations models forced with reduced CO_2 concentration, Peltier's (1994) ice-sheet reconstructions, and changes in orbital parameters. For the sea-surface temperatures (SSTs) two alternatives were given: (1) prescribed SSTs, taken from the CLIMAP dataset (CLIMAP 1981), or (2) computed SSTs from a slab ocean model with a prescribed ocean heat transport.

Valdes (2000) summarised PMIP1 simulations for various time intervals (21, 15, 9 and 6 kyr) for South America. The paper discusses several difficulties of the Paleo climate simulations arising from this experimental design. For South America that study mentions a caveat in PMIP1 simulations related to the inadequate representation of the Andes Cordillera, which affects a correct treatment of atmospheric circulation in this region. The prescribed SST experiments showed only moderate cooling over the continents and, in particular, anomalously low temperatures, compared to observations, over the southern tip of the continent which would have resulted from the apparent overestimation of sea-ice cover around Antarctica. The models also showed a weak increase of precipitation over the southern tip of South America, but the inter-model variability was very large. Past changes in the westerly circulation and the embedded storm tracks, both in the Northern and Southern Hemispheres have been discussed in various papers. Kageyama et al. (1999) showed that coarse resolution models cannot represent storm tracks in an accurate manner. Valdes (2000) reported that, for the LGM simulations, most models showed a poleward shift of the mean westerlies. This is consistent with results from a higher-resolution GCM simulation by Wyrwoll et al. (2000) that also showed a general poleward shift of the Southern Hemisphere storm tracks. Their results, however, show substantial regional differences, with a conspicuous poleward shift over the Australian sector, and an equatorward shift in the westerlies storm tracks in the vicinity of South America. More recent studies carried out with coupled AOGCMs still show ambiguous results with respect to the Southern Hemisphere westerly circulation, Kitoh et al. (2001) and Shin (2003) indicate a poleward shift in the surface westerlies, whereas a study by Kim et al. (2003) displays an equatorward shift. Results of a newer version of the CCSM3 model (Otto-Bliesner et al. 2006) indicates no shift in the position of the maximum westerlies during the LGM, but an increase in the intensity of the westerly circulation, as expressed by the surface wind stress.

In this paper we present results from four simulations conducted in the framework of the second phase of the Palaeoclimate Modelling Intercomparison Project (PMIP2), with identical forcings applied to all models. These simulations were carried out by state-of-the-art coupled GCMs, that include a dynamic ocean component, so that the responses of sea-ice, ocean and atmosphere are dynamically consistent, and hence it is expected that many of the problems in the previous generation of Palaeoclimate experiments will be addressed more appropriately. The aim of this paper is to report on the simulated changes in these state-of-the-art models and advance in the knowledge of a number of basic unanswered questions that linger in the palaeoclimate literature. These questions include: (1) Did the southern westerlies intensify/abate their velocity during the LGM?. (2) Did the westerlies widened, narrowed, or shifted latitudinally during the LGM?. (3) Did the storm

tracks embedded in the westerlies change during the LGM?. (4) Were changes in latitude and speed of the winds symmetrical over the major ocean basins of the southern Hemisphere?

Although we carried out analysis for the complete Southern Hemisphere and the four seasons, the discussion in the paper focuses on the summer (DJF) and winter (JJA) seasons.

2 Models and experiments

In this study we analyse four PMIP2 (Braconnot et al. 2007) coupled ocean–atmosphere models: the Hadley Centre HadCM3 model, the Japanese Model for Interdisciplinary Research on Climate MIROC3.2.2, the National Center for Atmospheric Research (NCAR) Community Climate System Model version 3 (CCSM3) model, and the Institute Pierre Simon Laplace Climate System Model, IPSL-CM4.

All models are fully coupled and include at least the following components: atmosphere, ocean, land surface and sea-ice. The HadCM3 model includes the MOSES II land surface scheme with 9 different possible surface types, a vegetation and a sea-ice model (for more details see Hewitt et al. 2003). The NCAR CCSM3 is a climate model whose atmospheric component (CAM3) is a spectral model, solved at T42 horizontal resolution. The land model uses the same grid as the atmospheric model and specified but multiple sub-grid land cover types (five types) and seven primary plant functional types. The ocean component (POP model) and the sea ice model use the same resolution, and includes sub-grid scale ice thickness (more information about CCSM3 can be found in Collins et al. 2006). We analysed the medium resolution MIROC3.2.2 model, which is a fully coupled model with the four aforementioned main components, in addition it has a river routing model, for more information see http://www.ccsr.u-tokyo.ac.jp/kyosei/hasumi/MIROC/tech-repo.pdf. Finally, the IPSL-CM4 uses the LDMZ atmospheric component and ORCA for its ocean component, it also includes a three layer sea-ice model (snow and 2 ice layers) and a land vegetation model with 12 plant functional types (for more information in: http://dods.ipsl.jussieu.fr/omamce/IPSLCM4/DocIPSLCM4/FILES/DocIPSLCM4. pdf). Table 1 gives some general characteristics of the atmospheric and oceanic components of these models. Results from other coupled GCMs run by PMIP2 for the LGM, with the required data, were not available for us at the time of this analysis.

We assessed the performance of all models using a control period, defined as Pre Industrial (PI) climate conditions, and LGM boundary conditions. The PMIP2 forcing of the LGM simulations includes the following three sources: changes in orbital parameters, differences in greenhouse gases concentrations, as well as different to present continental ice-sheet distribution, coastlines and topography. The ICE-5G ice-sheet reconstruction by Peltier (2004) is used as boundary condition with the corresponding changes in land-sea mask. However, vegetation remains unchanged relative to the control simulation. More information on the basic setup for these experiments can be found on the PMIP2 webpage (http://pmip2.lsce.ipsl.fr/).

The simulations for both experiments were run for long enough to allow the atmosphere and oceans reach quasi-equilibrium state to the specified boundary conditions and for trends to become small. For the LGM simulations HadCM3 started from the cold state of a previous coupled LGM simulation, whereas MIROC3.2.2 was initialised from modern conditions. CCSM3 uses a PI state to start the atmospheric component, whereas the ocean is initialised by applying the anomalies from a previous LGM simulation. IPSL-CM4 started from the Levitus conditions of a number of parameters (temperature, salinity, oxygen, etc) for the ocean (Levitus 1994 World Ocean Atlas) and an atmospheric state from a previous atmospheric GCM experiment. In this simulation, the deep ocean has not achieved complete equilibrium but the atmosphere and upper ocean characteristics are stable. We analysed the final 30–100 years of each simulation.

All variables used in this paper were monthly mean data, except for the evaluation of the storm tracks. For this we used daily sea level pressure data. Several indicators are commonly used to evaluate synoptic variability and associated storm tracks. In this study, we use a cyclone-tracking software that follows surface low pressure systems. The cyclone-tracking scheme was developed and implemented by Simmonds and Keay (2000), and references therein. In this scheme latitude–longitude data are transformed to a polar stereographic array centred around the pole (South

Table 1 PMIP2 coupled ocean–atmosphere models employed in this analysis

Model name	Atmosphere res lon × lat	Vertical levels	Ocean lon × lat	Vertical levels	Years used in analysis
HadCM3M2	3.75 × 2.5	19	1.25 × 1.25	19	100
MIROC3.2.2	2.8 × 2.8	20	1.4 × 1.4	43	30
CCSM3.0 ver beta14	1.4 × 1.4	26	~1 × 1	40	30
IPSL-CM4v1	3.75 × 2.5	19	2.4 × 2.4 cosϕ	31	100

Pole in this case). The low-finding routine tries to locate the position of the associated pressure minimum by iterative approximations. Full details are discussed in Simmonds and Murray (1999) and Simmonds et al. (1999).

3 Results

In this section we evaluate simulated temperature, sea level pressure, circulation, storm tracks, and precipitation. First, we assess the models performance against present day atmospheric reanalysis data (1961–1990 mean), and then we present differences between the LGM and control simulations. Although the control simulations were forced with PI greenhouse gas concentration, we will evaluate these runs with present day climatology for the remainder of the paper.

3.1 Temperature

Seasonal mean summer and winter surface air temperatures were compared with those from the NCEP/NCAR reanalysis (Kalnay et al. 1996), and shown in Fig. 1. All models show a cold bias over most grid points of the southern

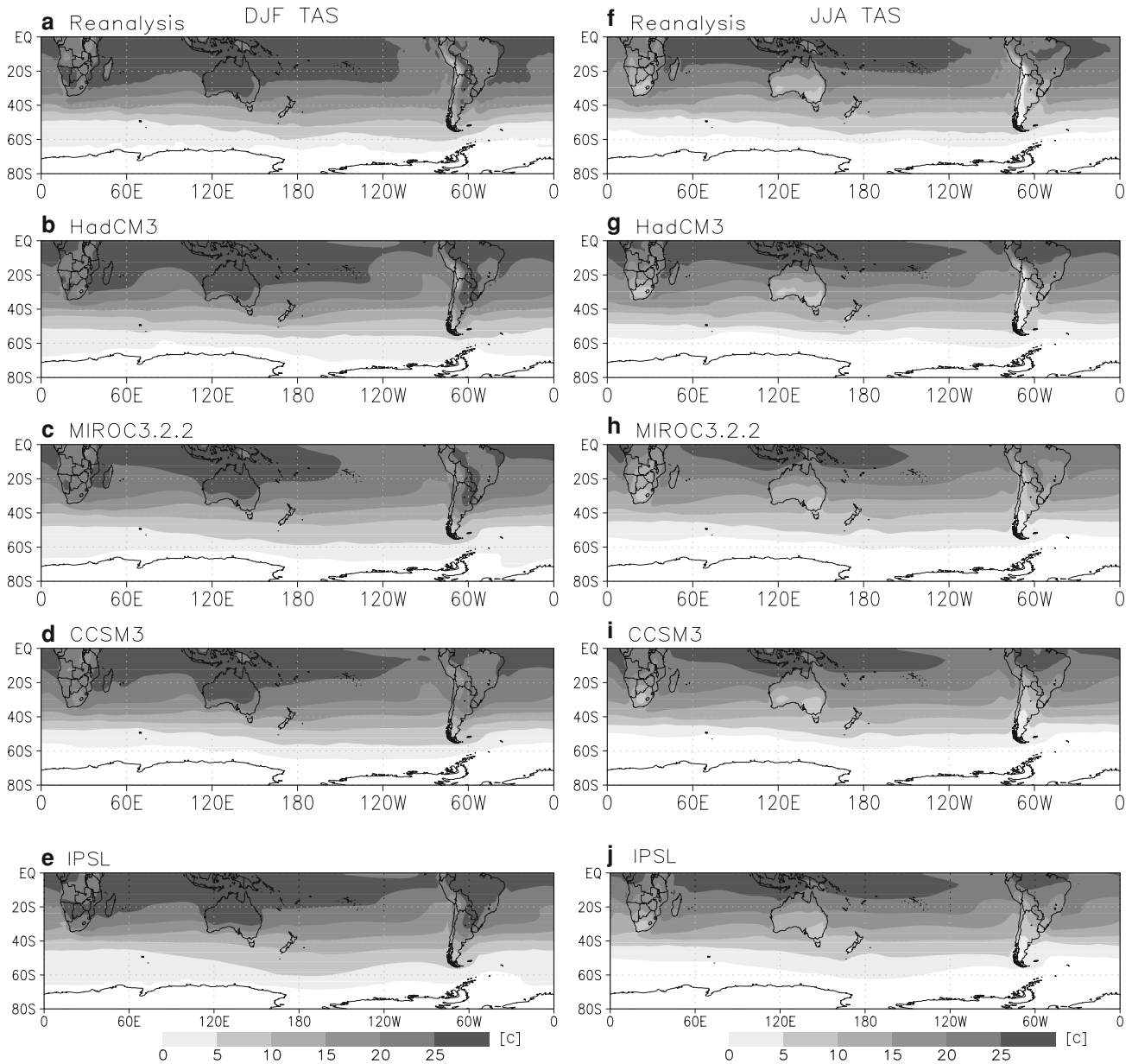

Fig. 1 Present day seasonal mean surface temperature fields for summer (*left column*) and winter (*right column*). From reanalysis (*top row*) and four models

oceans (ranging from 1° to 5°) in both seasons. Over the land masses the biases are less uniform and are season dependent, for example in summer (DJF) all models exhibit a cold bias over most of Australia (−2° to −3°) and Antarctica (−5° to −8°). Over South America, HadCM3 and IPSL simulate warmer temperatures (over 3°). In winter all models have a considerable warm bias over Antarctica (5°–8°), the western coast of South America (3°–5°) and parts of southern Africa (3°–5°), whereas Australia is well simulated. Although all models have biases in the surface temperatures, CCSM3 simulates largest and most uniformly colder temperatures compared to reanalysis over the southern ocean in summer and winter.

The above atmospheric surface temperature biases reflect similar biases in the underlying SSTs. Modelled SSTs were compared with a climatological SST dataset (Reynolds and Smith 1994, not shown). In summer and winter three models (except HadCM3) show a negative SST bias over most of the oceans, north of 50°S, and a positive bias at the western coast of Africa and South America, indicating that the upwelling regions are not well captured by the models. In summer all models, except CCSM3, simulate warmer SSTs around Antarctica. Overall HadCM3 tends to simulate a warmer Southern Ocean compared to observations.

The geographic distribution of the seasonal mean surface temperature changes between the LGM and present are shown in Fig. 2. For each model the seasonal differences between the LGM and PI simulations of summer and winter are shown. As expected, all models simulate, to different degrees, a colder climate for all seasons. The red and blue lines on the figures indicate the position of the area covered by 80% of sea-ice for PI and LGM, respectively. Next to each panel of temperature difference are profiles of the zonal mean meridional temperature gradient from 80°N to 80°S. Largest cooling is seen in the winter season over Antarctica and the surrounding oceans, which were covered by extensive sea-ice during the LGM (see blue lines in Fig. 2). Of the four models, CCSM3 produces the largest cooling, ranging from 3° to 5°C over the continents (Australia and Southern South America) to over 15°C over Antarctica. IPSL simulates the least cooling, and mainly over the continents, similar to MIROC3.2.2. The surface temperature and sea-ice changes are consistent. From the four models, CCSM3 simulates the largest sea-ice cover extent during the LGM, and IPSL the minimum.

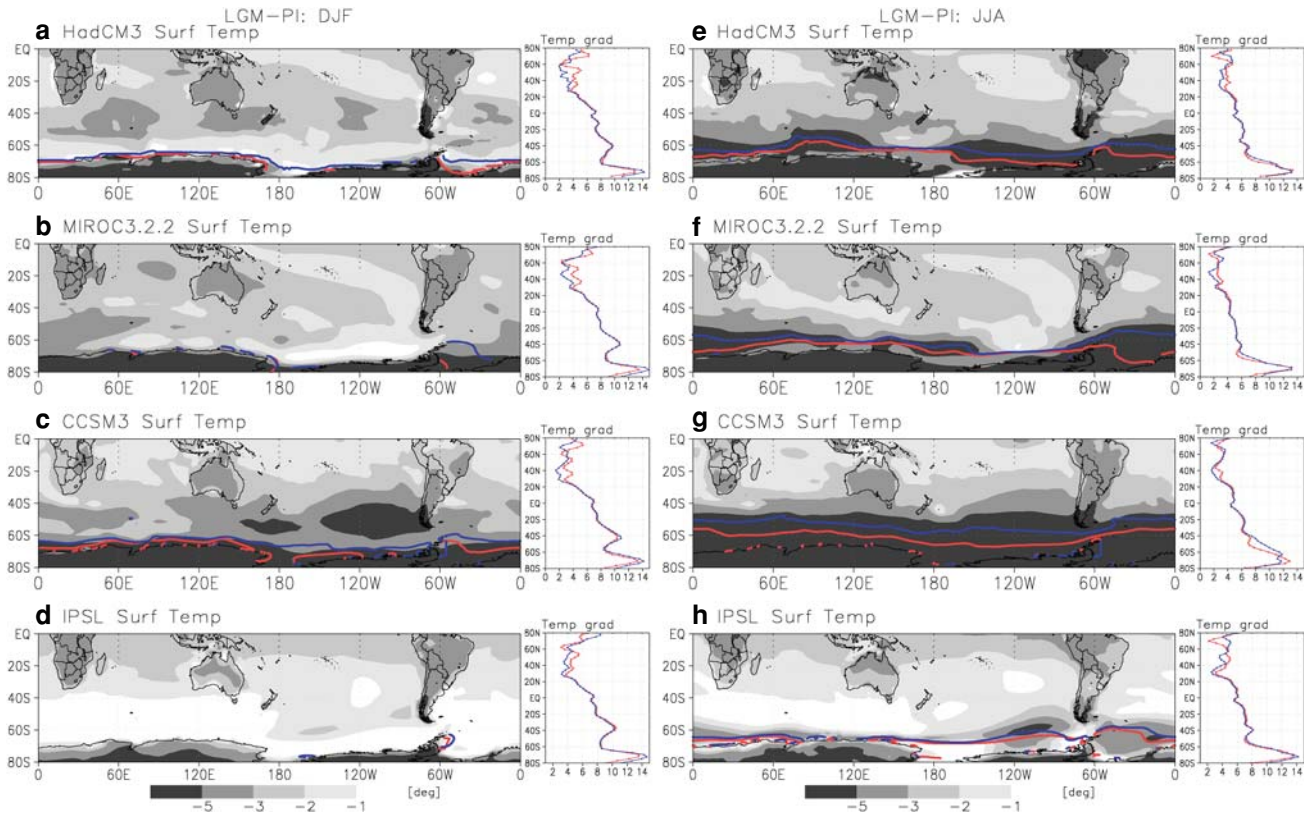

Fig. 2 Seasonal mean surface temperature changes LGM-PI for summer (*left panels*) and winter (*right panels*) of the four models. The *red and blue lines* represents the position of the 80% sea-ice cover during PI and LGM, respectively. The profiles at the right of each panel correspond to the zonal mean meridional surface temperature gradient, from 80°N to 80°S. *Red line* for PI and *blue* for LGM

Temperature changes are strongest at high latitude over land or sea-ice, but there is much less polar amplification of the cooling than for the northern hemisphere (Braconnot et al. 2007). In fact, over much of the ocean the temperature changes are rather homogeneous (except for CCSM3). So, the meridional temperature gradients that are a driver of the atmospheric circulation should not change a lot (compared to the northern hemisphere), as seen in the profiles of Fig. 2, except south of about 70°S and hence the circulation main structures should be quite stable. Finally, a large sensitivity in the sea-ice response, in an already cold CCSM3 model, can probably partly explain the large temperature and sea-ice cover response to the LGM forcings in this model.

3.2 Sea level pressure

We found considerable changes in sea level pressure (SLP), associated to changes in surface temperature and sea-ice cover during the LGM. Figure 3 shows the seasonal mean SLP for summer (DJF) and winter (JJA) from reanalysis (top panels) and the PI simulations of the four models. In general terms, the subtropical anticyclones are well simulated in their intensity and position in all four

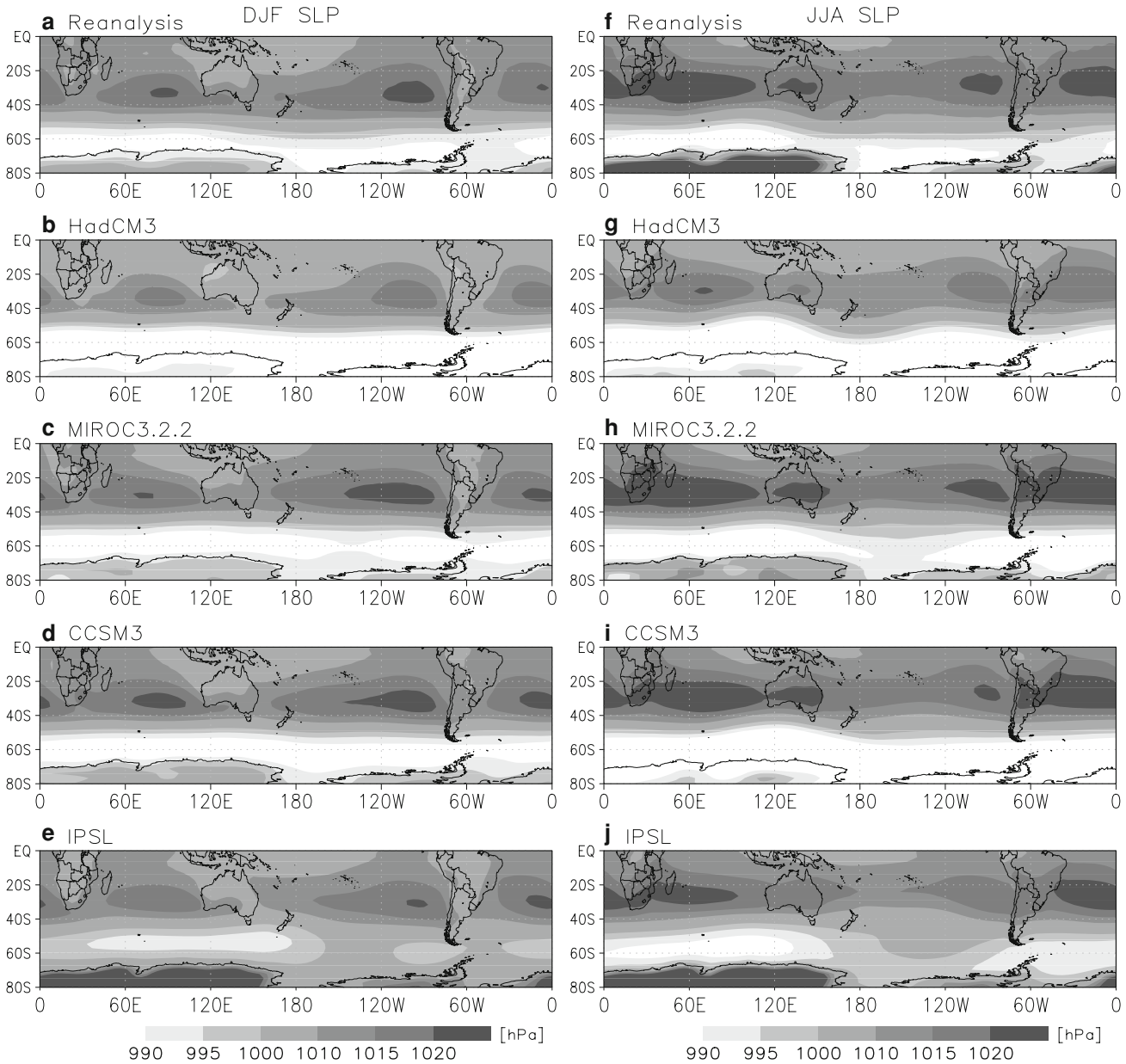

Fig. 3 Present day seasonal mean sea level pressure fields for summer (*left column*) and winter (*right column*). From reanalysis (*top row*) and four models

models. HadCM3, MIROC3.2.2 and CCSM3 simulate a more intense circumpolar trough between 40° and 50°S with larger SLP gradients. IPSL simulates a weaker and less circumpolar trough and exhibits anomalously high pressure fields over Antarctica compared to reanalysis. HadCM3 simulates weaker anticyclones in all seasons (about 5 hPa lower).

For the LGM, HadCM3, MIROC3.2.2 and IPSL simulate higher SLP values in all seasons over the Southern Hemisphere, with the largest differences occurring during summer over Antarctica. CCSM3 shows the opposite pattern, with a large decrease in SLP over the southern oceans and Antarctica (not shown).

As the winds are related to SLP gradients, Fig. 4 shows the meridional gradient of SLP averaged over the three main ocean basins. The SLP gradient from NCEP/NCAR reanalysis is included for reference (black line). The largest differences with respect to reanalysis are found in the Pacific and Atlantic oceans and during winter. MIROC3.2.2 and IPSL tend to shift the latitude of maximum gradients further equatorward and CCSM3 tends to overestimate the maximum SLP gradients, but at a correct latitude. In general, HadCM3 simulates this feature best.

Comparing the gradients between PI and LGM simulations (full lines against dotted lines), HadCM3 simulates lower gradients in all basins for the LGM, particularly in the South Pacific ocean. This feature is reflected in weaker near surface winds. MIROC3.2.2 shows a mixed response, for example, in the South Pacific ocean the model simulates decreased gradients in summer and somewhat increased and poleward shifted gradients in winter. CCSM3 simulates consistently small increases and poleward shifted gradients, especially in winter in the South Pacific and South Atlantic oceans. IPSL simulates decreased SLP gradients and also an equatorward shift in these gradients in all basins and seasons. Notice from Fig. 4 that the biases between the PI and reanalysis are often larger that the LGM–PI anomalies.

3.3 Circulation

The entire Southern Hemisphere between 30° and 70°S is under the year-long influence of the westerly winds from

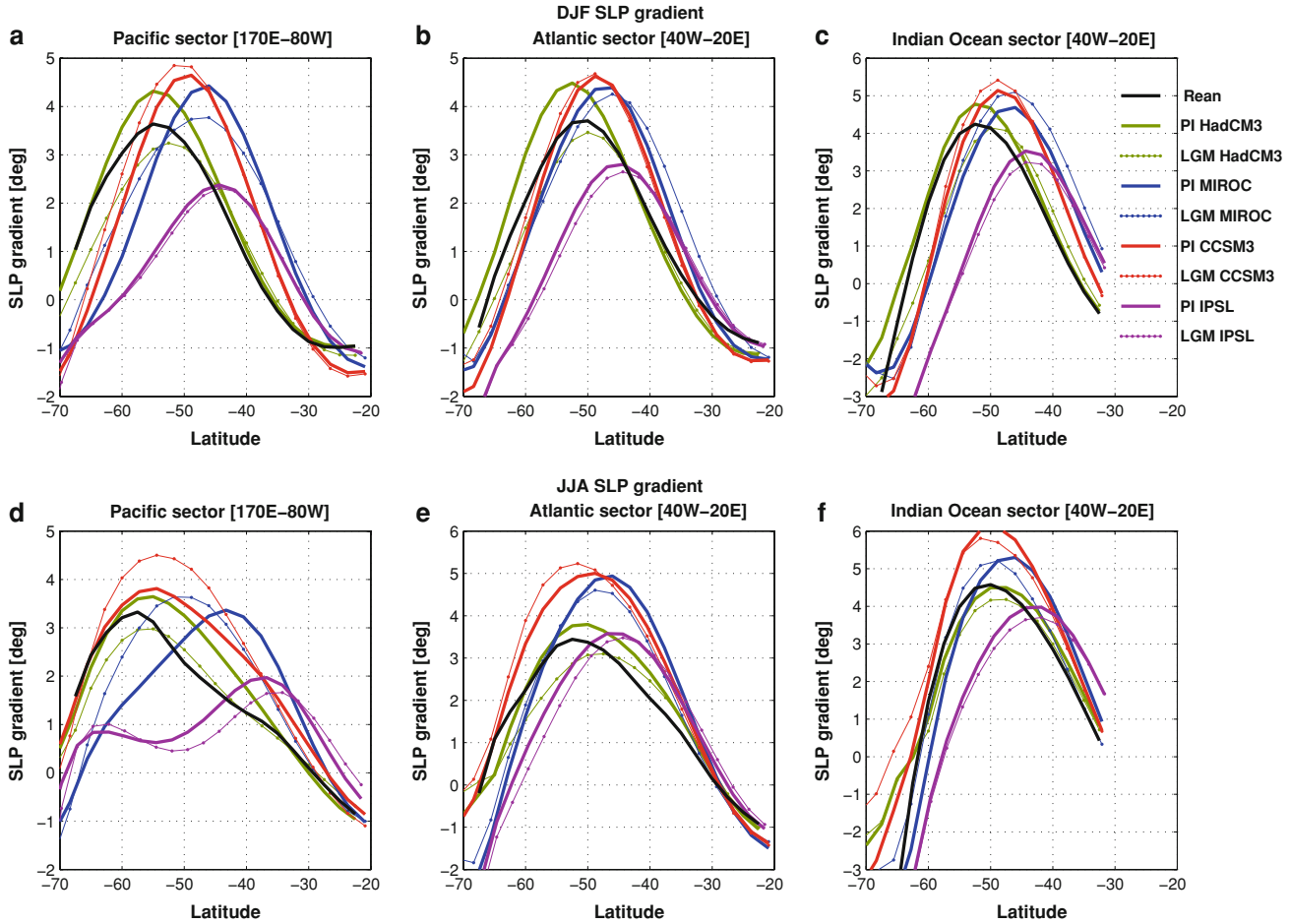

Fig. 4 Meridional sea level pressure gradients averaged over the three main ocean basins (South Pacific, South Atlantic and Indian oceans). *Black* NCEP/NCAR reanalysis, *green* HadCM3, *blue* MIROC3.2.2, *red* CCSM3, *purple* IPSL. *Full lines* PI and *dotted lines* LGM

the surface to the tropopause. In the upper troposphere, the westerlies structure around the subtropical jet stream (STJ) and the subpolar jet stream (SPJ), both with distinct seasonal evolution in extent and strength, as well as vertical structure. Figure 5 shows the seasonal mean zonal winds at the near surface (925 hPa) for summer (left panels) and winter (right panels) from NCEP/NCAR reanalysis (top row) and the four models, for reference, the blue line represent the latitude of maximum wind speed of the NCEP/NCAR reanalysis.

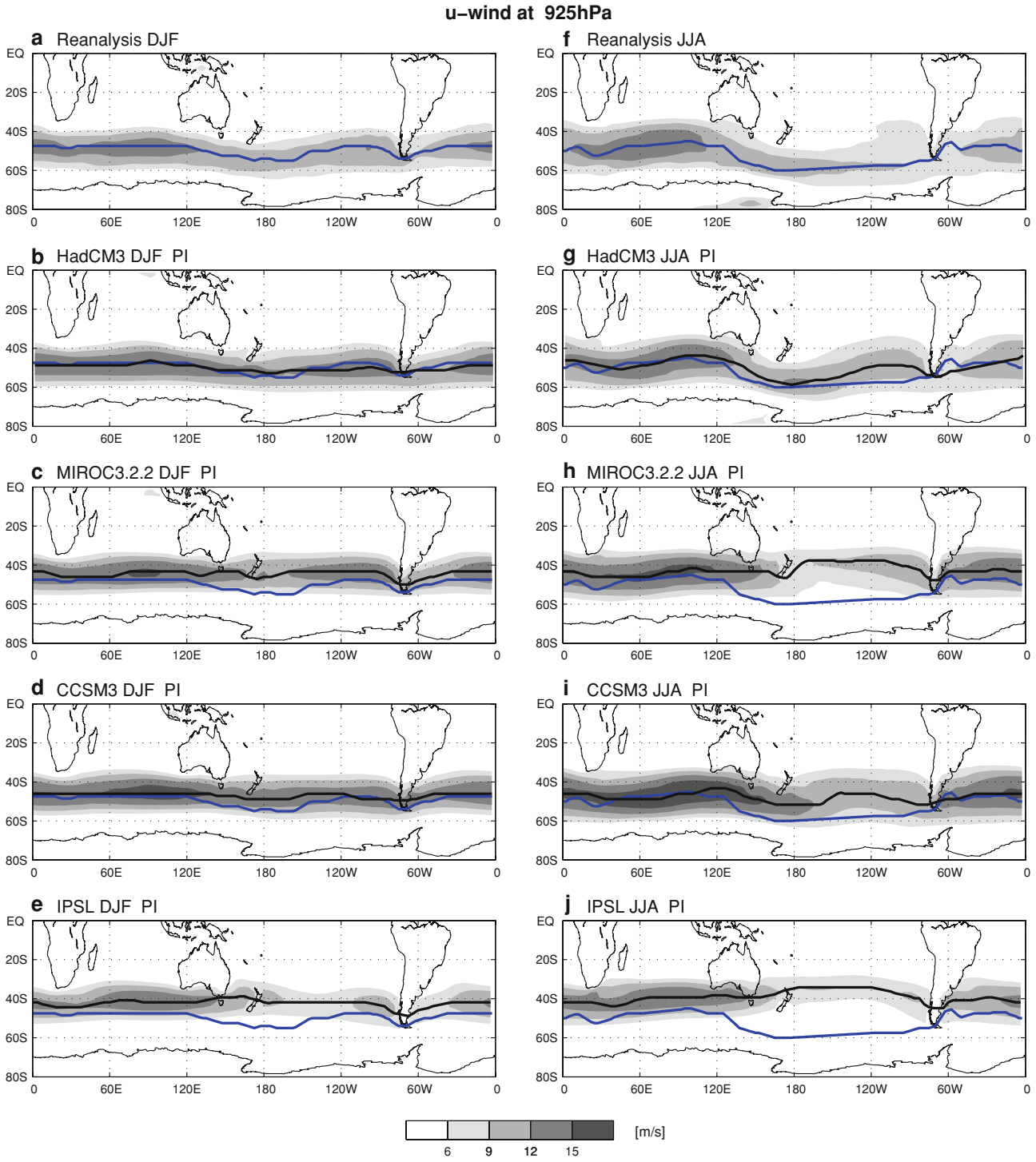

Fig. 5 Zonal winds at 925 hPa. *Top rows* from NCEP/NCAR reanalysis, following rows of the four models, during summer (*left panels*) and winter (*right panels*). *Black line* latitude of maximum wind speed, *blue line* latitude of maximum wind speed from NCEP/NCAR reanalysis

Near surface westerly winds are present between 30° and 70°S, with strongest winds centred at around 50°S. This band of the westerly winds corresponds to the near surface extent of the SPJ that has its core region at higher altitudes. Strongest winds are present over the South Atlantic and Indian oceans and weakest over the South Pacific ocean. The annual cycle over the South Atlantic and Indian oceans is marked by a maximum in autumn (SON) and winter (JJA) and minimum during summer (DJF). Over the Pacific ocean the maximum occurs in spring (SON) and summer (DJF) and the minimum in winter (JJA).

Figure 6 shows the same as Fig. 5, but for 200 hPa. The upper tropospheric winds are dominated by both the STJ and SPJ streams. The core region of the STJ is located over

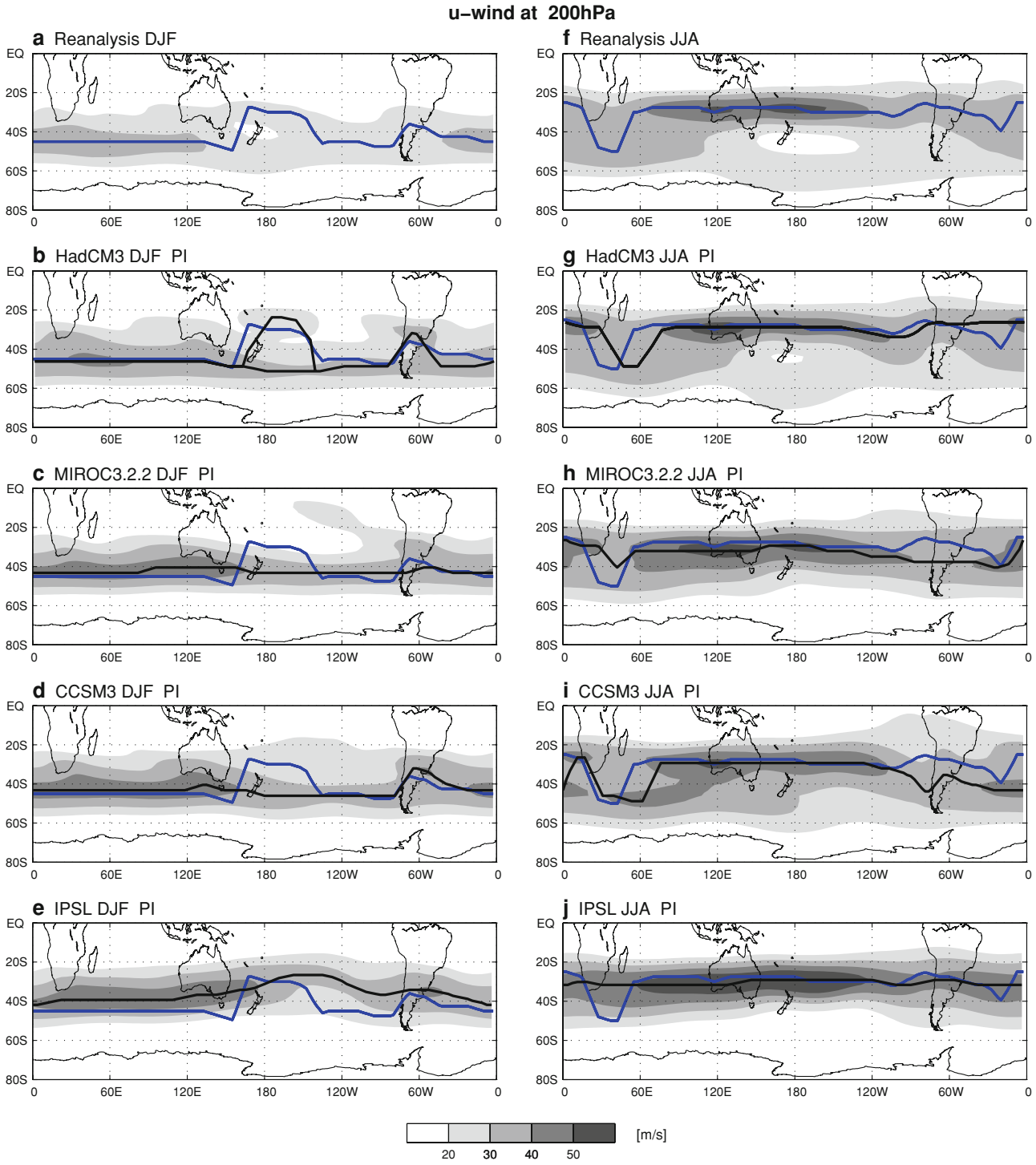

Fig. 6 Same as Fig. 5 but for 200 hPa

Australia and the western South Pacific ocean. The STJ has a marked annual cycle, having its maximum strength in JJA and almost disappearing in DJF. In contrast the annual cycle of the SPJ exhibits more modest changes, it is most intense and circumpolar in summer, when it is the dominant jet in the Southern Hemisphere, and weakened during winter and spring. As to the longitudinal extent, its core region is over the South Atlantic and Indian oceans at ~50°S. During winter, when the STJ intensifies north of the SPJ the well known double jet structure in the upper troposphere develops over the Indian and South Pacific oceans.

In Fig. 5 three models, except HadCM3, simulate the position of the maximum wind speed further equatorward than reanalysis, especially during winter (right panels). Additionally, the intensity is overestimated by the models, except IPSL, especially over the Indian ocean. At 200 hPa (Fig. 6) MIROC3.2.2, CCSM3 and IPSL fail to reproduce the double jet structure over the Pacific ocean in winter, underestimating the subpolar jet. The simulation of the subtropical jet is well captured by the models, IPSL overestimates the jet speed. In summer all models overestimate the SPJ and all, except HadCM3, shift the core of the jet further equatorward (40°–45°S instead of 50°S). HadCM3 reproduces the near surface and upper tropospheric circulation the best.

With respect to the circulation biases in the models, we note that for instance the equatorward bias in maximum near surface winds in the models are consistent with the equatorward shift in the maximum SLP gradients seen in Fig. 4. The biases in the upper level circulation can be explained by the tropospheric thermal structure in the models. Through the thermal wind equation the vertical wind gradient (i.e. jets) is related to the meridional temperature gradients. The Southern Hemisphere tropospheric temperatures, as seen in reanalysis, show strong gradients south of 70°S all year long (not shown). In addition, maximum gradients are found throughout the troposphere between 30° and 50°S. The maximum gradients vary throughout the year and, depending on the region, in a similar way as the already described evolution of the SPJ and STJ. Inspection of the temperature structure in the models and comparison with reanalysis (not shown) show a clear correspondence between the position and intensity of the temperature gradients, and the position and intensity of the SPJ and STJ.

When comparing the PI and LGM simulations in Figs. 7 and 8 (as well as in Figs. 9, 10, that show the difference fields), it is evident that the overall position and annual cycle of the maximum wind speeds do not change significantly. Only HadCM3 shows a modest general equatorward shift at the LGM in summer at both levels (compare black against red lines), and IPSL simulates a slight equatorward shift at the near surface in both seasons and a poleward shift in the upper troposphere over the south Pacific ocean.

Figures 9 and 10 show the differences between the LGM and PI simulations of the seasonal mean near surface and upper level zonal winds for the four models, respectively. In winter, these figures show that, three out of four models, indicate a decrease in the strength of the winds at 200 hPa (SPJ and STJ), as well as at the near surface. The exception is CCSM3, that shows a intensification of the SPJ and winds at the near surface. For the summer season the observed changes are smaller, but with a clear weakening of the SPJ. The stronger winds in CCSM3 are coherent with the larger SLP gradients simulated by the model in this region (Fig. 4) and the larger surface temperature and sea-ice response to LGM conditions. These features produce a larger meridional temperature gradient than in the other models (see profiles in Fig. 2). The other three models simulate decreased SLP gradients that are consistent with a weakened near surface circulation. Again, inspection of the tropospheric temperature reveals that, although there is an overall cooling of the troposphere in the models, this cooling does not increase the temperature gradients, as seen in zonal profiles of Fig. 2. HadCM3, MIROC3.2.2 and IPSL illustrate this point by showing a decrease in SLP gradients and weakened atmospheric circulation. One exception is the atmosphere south of 70°S, where the already large temperature gradients in the PI simulations are further enhanced in all LGM simulations.

Most noticeable in Fig. 9 is that the magnitude of the observed changes in near surface circulation are larger in winter than in summer, except in HadCM3, that shows significant differences in both seasons. During winter there are important regional heterogeneities, so that largest changes occur over the Pacific ocean. More specifically, for the winter season, HadCM3, MIROC3.2.2 and IPSL show similar patterns in the difference fields. The zonal band between 40° and 60°S shows decreased westerly winds in the LGM compared to PI, especially in the South Pacific region, and stronger winds north of 35°S in the same region. CCSM3 simulates the opposite pattern. In summer, HadCM3 shows a very longitudinally homogeneous band between 45° and 60°S of decreased westerly winds, and stronger winds north of this band. This is also seen, to a lesser degree in IPSL. The other models show less zonally symmetric patterns. MIROC3.2.2 and CCSM3 indicate somewhat stronger winds in a zonal band between 50° and 70°S.

At 200 hPa (Fig. 10) in summer, HadCM3 simulates a zonal band of weaker winds in the SPJ region (50°–60°S) and a narrow band of stronger winds north and south of this latitude. The other models show a less clear pattern,

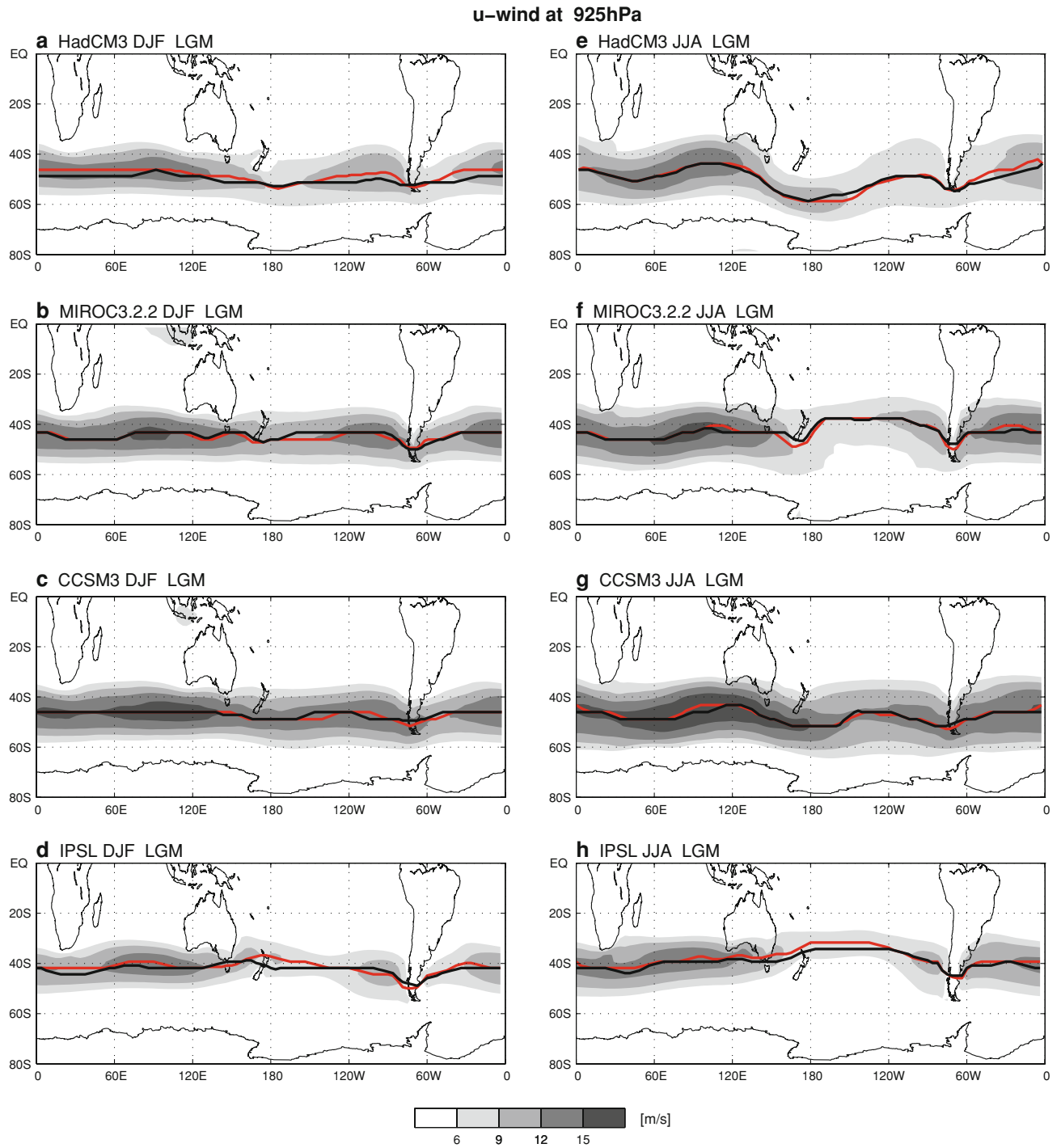

Fig. 7 LGM zonal winds at 925 hPa of the four models during summer (*left panels*) and winter (*right panels*). *Black line* latitude of maximum wind speed from PI simulation. *Red line* latitude of maximum wind speed of LGM simulation

with somewhat stronger winds from about 60° to 70°S and weaker north of this latitude. For winter HadCM3, MIROC3.2.2 and IPSL tend to agree, as for the low level winds, with decreased westerly flow in the zonal band 20° and 50°S, CCSM3, shows decreased winds north of 40°S and a strong increase south of this latitude, especially over the Pacific ocean. We note that the patterns of the difference fields arises from a general decrease or increase of wind strength rather than a significant shift (either equator or poleward) of the core of the jet streams or latitude of maximum wind speeds, as discussed previously.

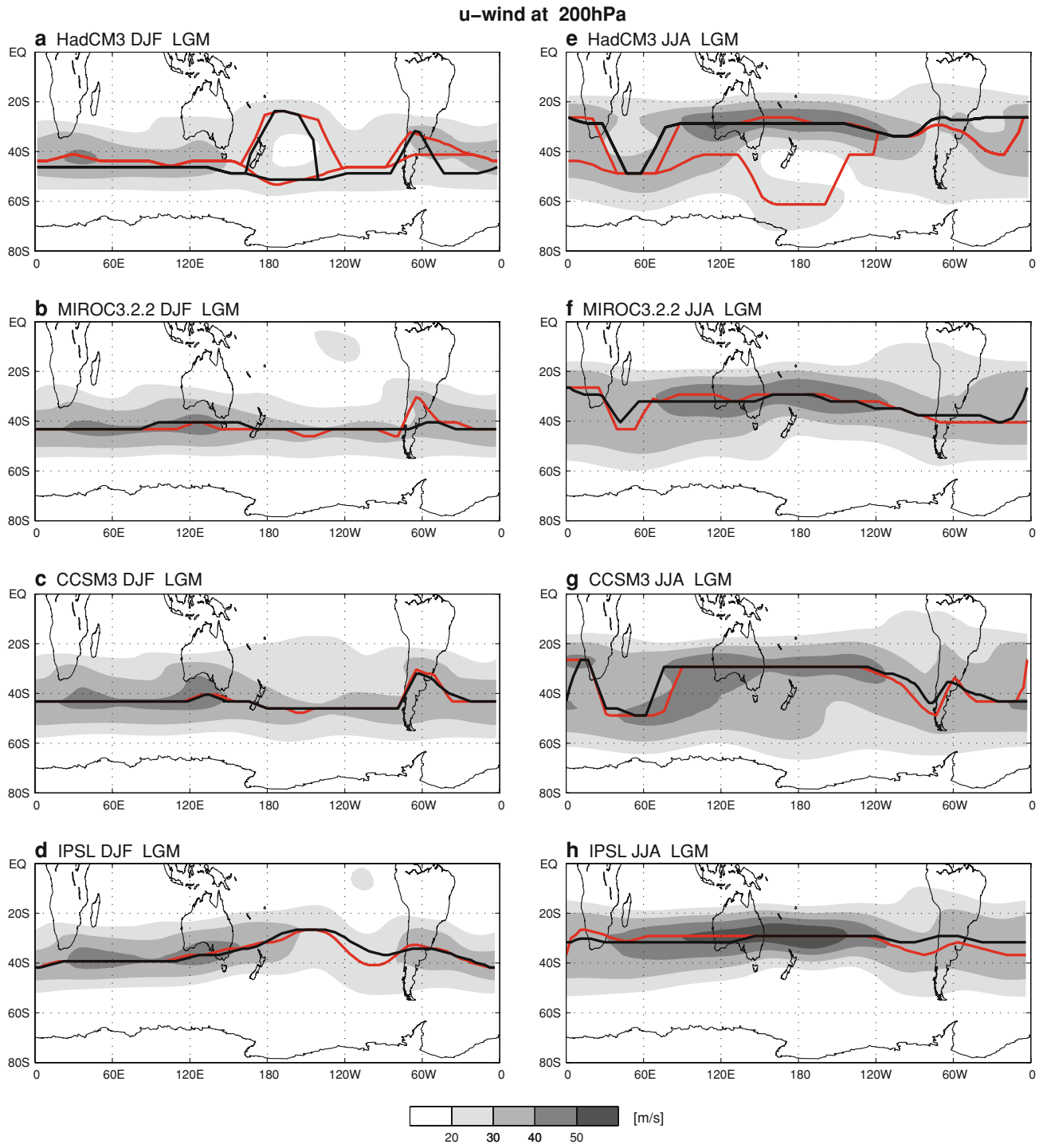

Fig. 8 Same as Fig. 7 but for 200 hPa

3.4 Storm tracks

Atmospheric variability responsible for much of the weather in the midlatitudes arises primarily from the passage of cyclones and anticyclones and their associated frontal systems. Consequently, past changes in the westerly storm tracks bear on precipitation changes during the LGM, as most of the winter precipitation in midlatitudes is of frontal origin. This is the case in western South America, the southern limit of Australia, and New Zealand in winter. In addition, orographic features enhance the precipitation in western Patagonia and the western slopes of New Zealand's south Island. In the Southern Hemisphere these systems are embedded in the westerly flow, and they are

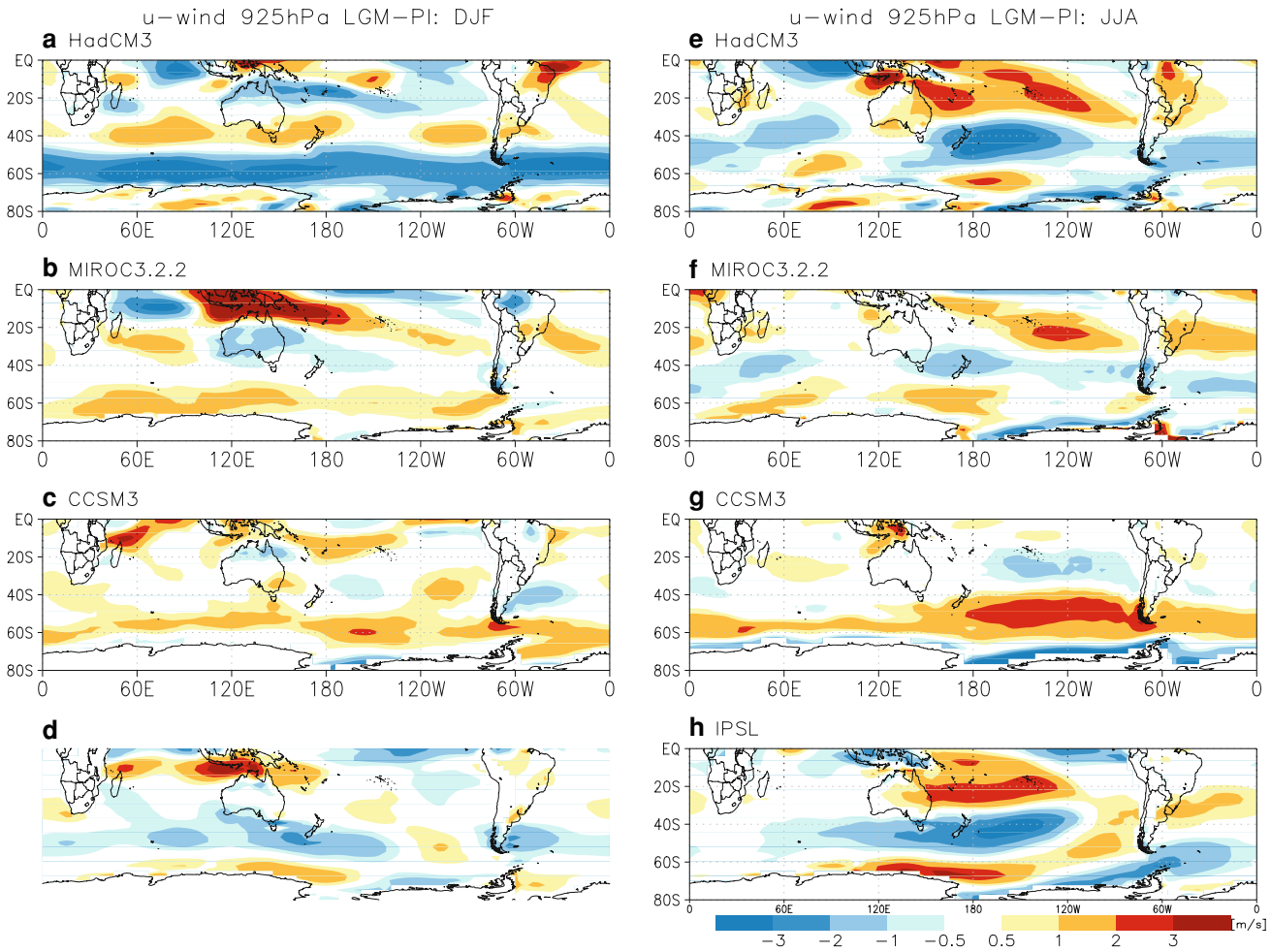

Fig. 9 LGM-PI 925 hPa winds for summer (*left column*) and winter (*right column*) for the four models

expected to differ between the LGM and present, as a consequence of changes in the mean westerly circulation discussed in the previous section.

First, we used daily sea level pressure data to track cyclones during the 30 year period of the control simulations and compared those results with the cyclone density found in NCEP/NCAR reanalysis sea level pressure. Figure 11 shows the seasonal mean cyclone density (the mean number of systems found in a 10^3 (deg lat)^2 area) for the Southern Hemisphere found by the tracking software in 30 years of daily SLP data, for summer (left panels) and winter (right panels) from the NCEP/NCAR reanalysis (top row) and the four models. The figure shows the well known maximum density at high latitudes. In winter, when zonal asymmetries are largest, a secondary storm track at midlatitudes is especially pronounced in the Pacific sector. The top row of this figure can be compared with Fig. 4 from Simmonds and Keay (2000), where they used 6-hourly ERA-40 data.

Comparing the models with the observations in Fig. 11, the first we observe is that the models simulate smaller cyclone density than the observations. Disregarding this bias, we see that HadCM3 annual density as well as the seasonal densities compares best with the NCEP/NCAR reanalysis. The highest density is found around Antarctica with maximum values in the Atlantic and Indian oceans. The density by seasons also reproduce the more symmetric summer activity (DJF) and the more zonally asymmetric winter season (JJA) with higher cyclone activity in the midlatitudes of the Australian and Pacific ocean sectors. The other three models tend to underestimate the secondary, midlatitude storm track present during winter over the Pacific ocean. Additionally, IPSL simulates the primary circumpolar storm track further equatorward than reanalysis.

After this first analysis we applied the cyclone tracking procedure to calculate the cyclone tracks for the LGM simulations. The differences between LGM and PI system density are shown in Fig. 12. Overall there are not many common patterns in the difference field. Except over the Pacific ocean, where we see positive changes between 30° and 45°S, negative changes between 50° and 60°S, and

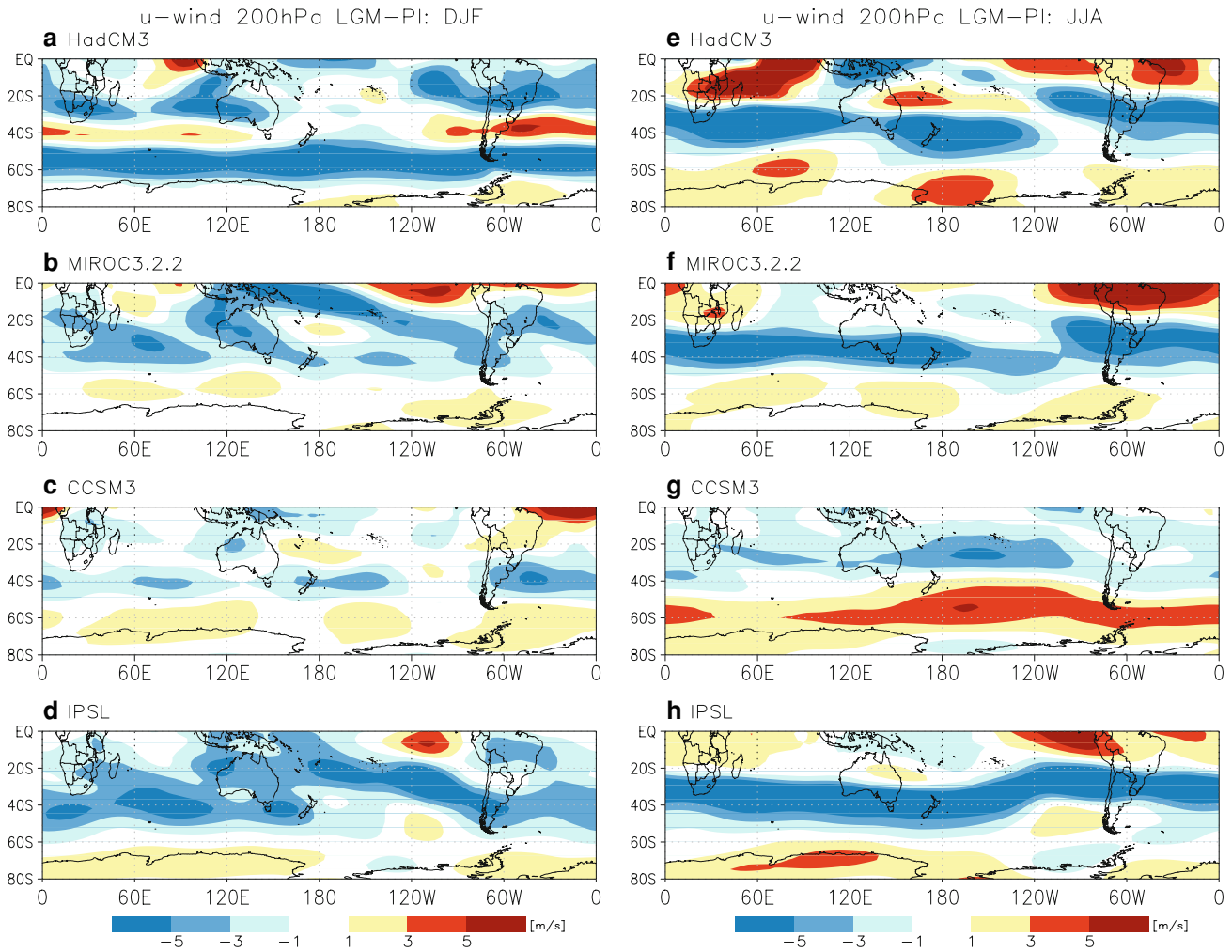

Fig. 10 LGM-PI 200 hPa winds for summer (*left column*) and winter (*right column*) for the four models

again positive changes between 60° and 75°S in summer and winter.

3.5 Precipitation

We analysed the precipitation changes associated with the atmospheric circulation and temperatures simulated in the LGM experiments. As models differ in their ability in simulating present day precipitation over the different regions first we compare the precipitation of the PI simulation with a global precipitation estimate. Figure 13 shows the seasonal mean precipitation distribution in the Southern Hemisphere from the CMAP gridded precipitation estimate (Xie and Arkin 1996) (top row) and the PI simulations of the four models. In summer the data show a well defined South Pacific Convergence Zone (SPCZ) starting at around the equator and 150°E trending towards the south east to about 40°S and 120°W. Over South America and extending into the South Atlantic is the South Atlantic Convergence Zone (SACZ). In winter the SPCZ is still present although diminished, whereas over the South American continent a precipitation minimum is seen. Over the South Atlantic ocean a precipitation band is still possible to observe in JJA. Some systematic errors in the simulation of the precipitation are found. In summer, all models, except IPSL, overestimate the precipitation over Australia. The SPCZ is not as well defined as in the CMAP data, except HadCM3, that has a reasonably well defined SPCZ as well as SACZ. In addition, MIROC3.2.2 and CCSM3 simulate the Intertropical Convergence Zone too far south.

Figure 14 shows the precipitation differences (LGM–PI) and the zonal mean precipitable water (absolute values) for PI and LGM, for summer (left panels) and winter (right panels) in the four models. Some of the common patterns include a decrease in precipitation over the entire zonal band south of 55°S in summer and south of 40°S in winter, as well as drier conditions compared to PI in eastern Australia during summer. There is also agreement over slightly wetter conditions during the LGM in the southwestern tip of Australia during winter. In South America

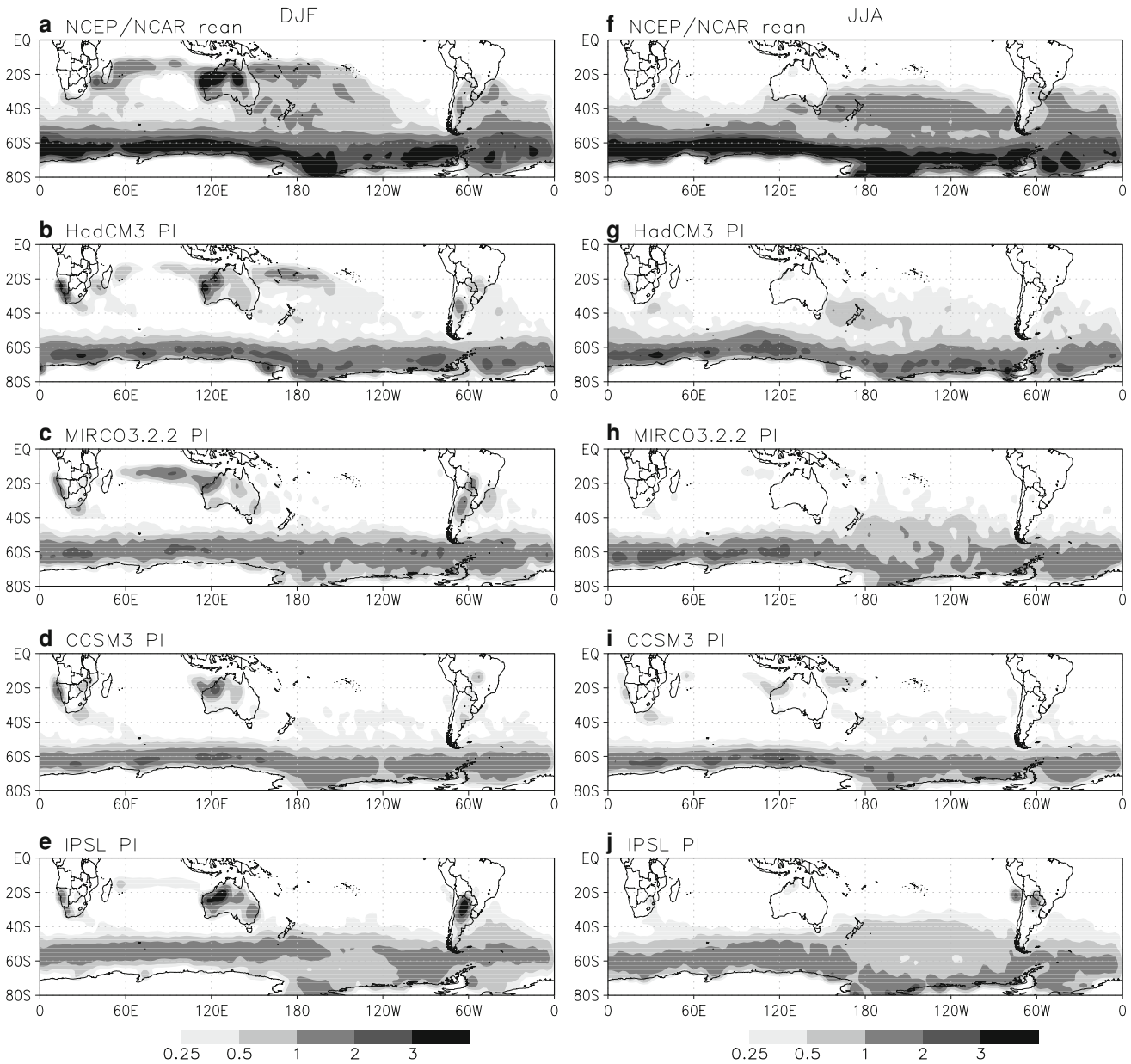

Fig. 11 Cyclone density (the mean number of systems found in a 10^3 (deg lat)^2 area)^2) for summer (*left panels*) and winter (*right panels*) from NCEP/NCAR reanalysis and models for PI

during winter, HadCM3 and MIROC3.2.2 show an increase of precipitation north 40°S along the western coast, and a decrease to the south of this latitude, CCSM3 simulates a decrease and IPSL an increase. On the lee-side of the Andes, all models indicate decreased precipitation. For the summer season the situation on the lee side of the Andes is similar to winter. At the western coast, all models, except CCSM3, indicate positive differences over most of the region. CCSM3 simulates negative changes over all the coastal region. For Australia there is much disagreement among models. HadCM3 indicates drier conditions over most of the continent for all seasons, except in the southwestern corner in winter (JJA). MIROC3.2.2 simulates decreases precipitation in summer and increased in winter. CCSM3 predicts mixed increases and decreases depending on the season and IPSL simulates drier conditions and winter and wetter in summer. As was already mentioned, the four models agree in predicting drier conditions in south western Australia. Over New Zealand all models indicate drier conditions in summer, except IPSL that predicts somewhat wetter conditions over North Island, and all models, except CCSM3, indicate drier conditions in winter. Over Africa more agreement is seen, with a tendency of increased precipitation during the LGM

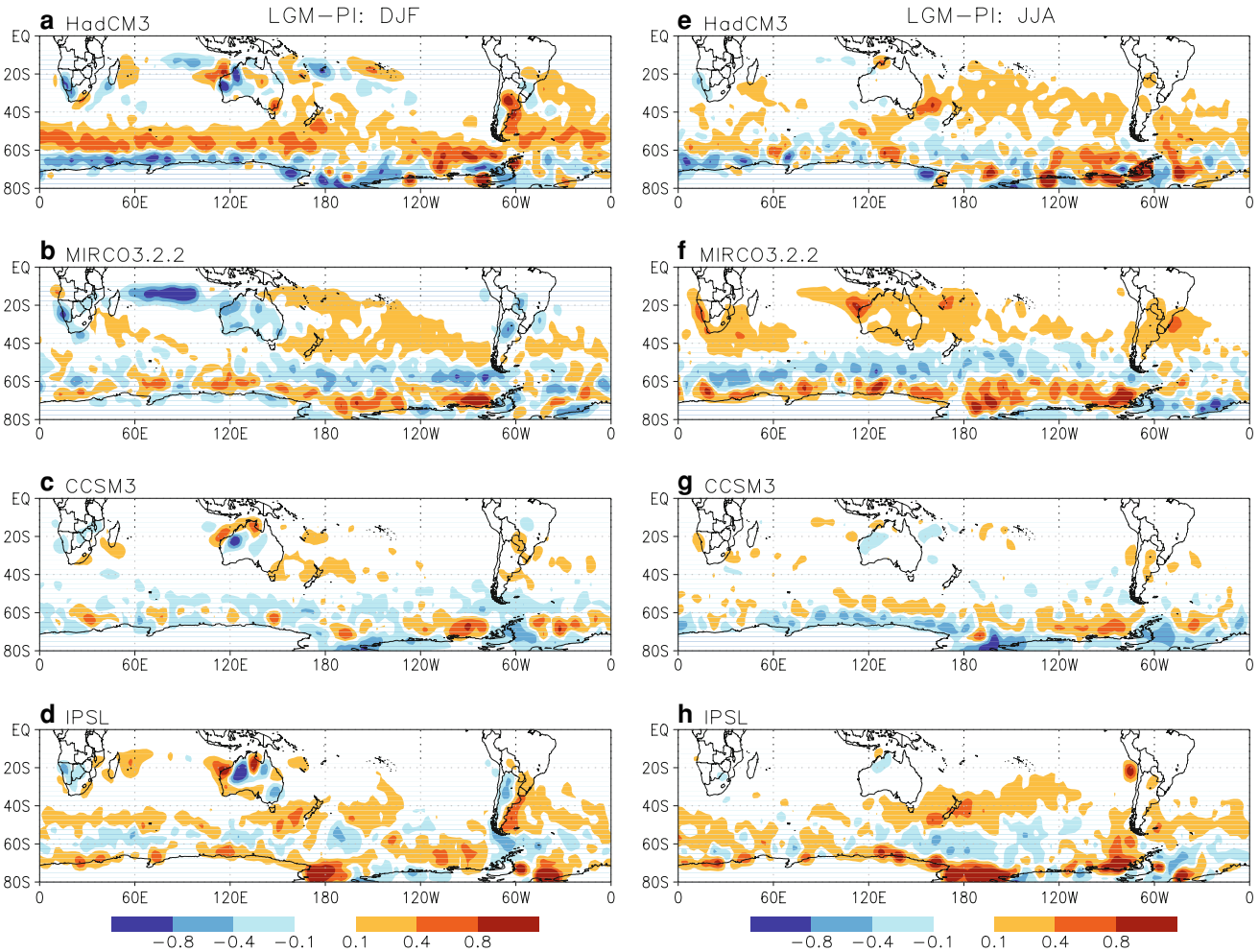

Fig. 12 Model cyclone density LGM-PI for summer (*left panels*) and winter (*right panels*)

compared to pre industrial conditions, especially in winter. In summer HadCM3, MIROC3.2.2 and IPSL simulate increased and CCSM3 decreased precipitation.

Some of the precipitation changes described above over the land masses reflect shifts and changes of the convergence zones during the LGM. In summer MIROC3.2.2 and HadCM3 simulate a stronger SACZ and a westward shift of the SPCZ. In winter the SPCZ is stronger than PI and displaced further to the west. CCSM3 and IPSL tend to simulate diminished convergence zones in the South Pacific as in the South Atlantic oceans.

In the midlatitudes, in general the precipitation changes are consistent with circulation changes, in the sense that regions with increased near surface winds coincide with regions of increased precipitation and vice-versa. This is the case in HadCM3, MIROC3.2.2 and IPSL. CCSM3 however, simulates large regions of increased zonal winds and decreased precipitation. Presumably, a factor responsible for the decreased precipitation is the overall drying of the atmosphere during the LGM, as seen in latitudinal profiles of precipitable water in Fig. 14. Atmospheric precipitable water was roughly 50% less than PI south of 70°S, 50–70% less south of 60°S and 80–90% less in midlatitudes (larger drying is found during winter).

3.6 Atmospheric influence on the Southern Ocean

As stated in the introduction, Toggweiler et al. (2006) discussed the role of the midlatitude westerlies in glacial-interglacial transitions, arguing that equatorward-shifted westerlies and diminished surface wind-stress during glacials would influence dissolved and atmospheric CO_2 concentrations and reduced ocean overturning in the Southern Ocean. Sigman and Boyle (2000) proposed that a decrease in the polar upwelling of CO_2- and nutrient-enriched deep waters, in conjunction with expanded sea-ice would lead to increased stratification of the glacial Southern Ocean. This physical mechanism, in conjunction with a biological mechanism that involves higher nutrient

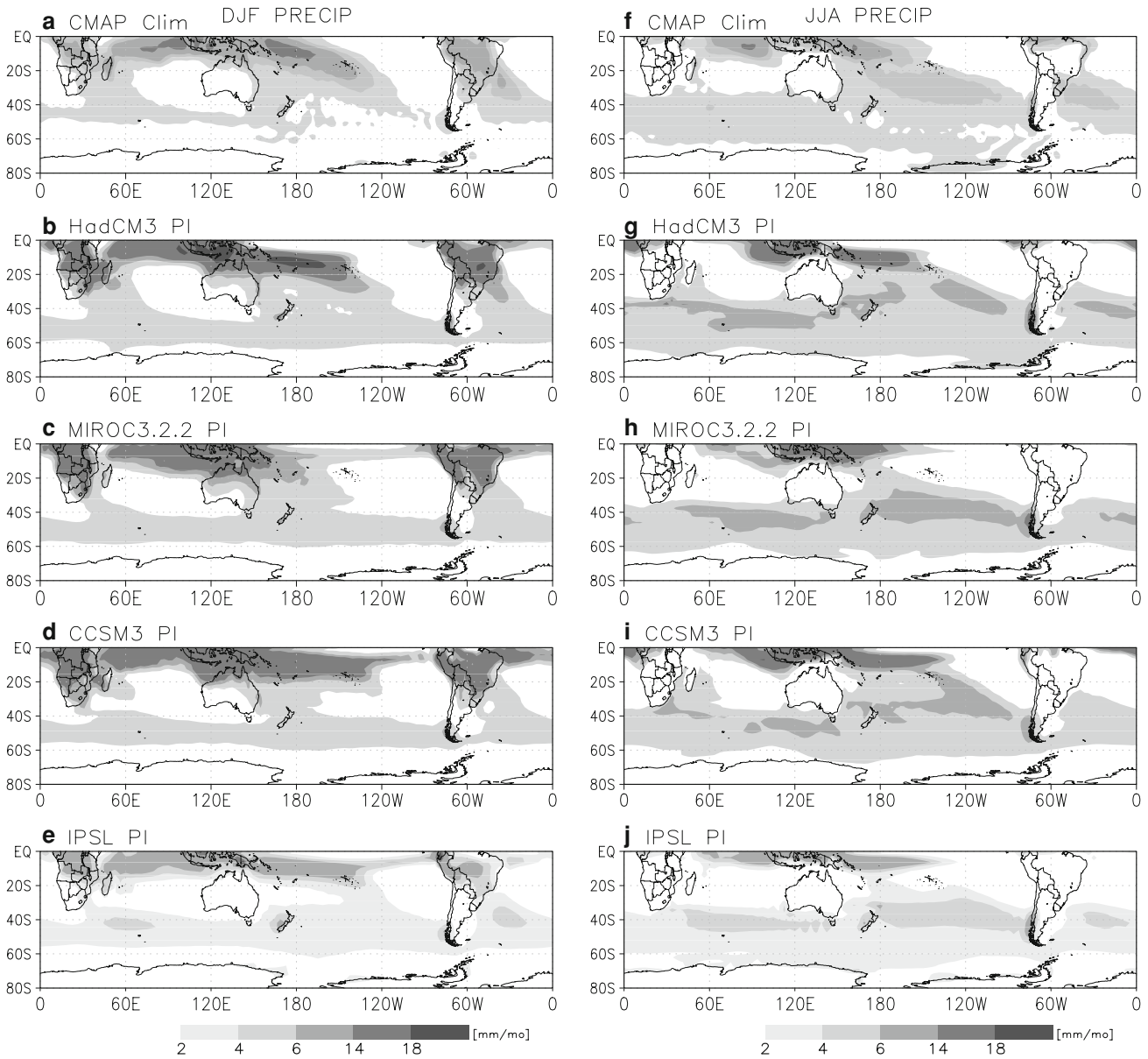

Fig. 13 Seasonal mean precipitation comparison for summer (*left panels*) and winter (*right panels*), from CMAP gridded analysis (*top row*) and the four models

utilisation of upwelled intermediate waters, and mediated by increased deposition of iron-rich dust on the surface of the sub-antarctic ocean, have the potential of lowering CO_2 concentrations of the glacial atmosphere.

Caring out a complete analysis of the ocean circulation is outside the scoop of the paper. However, in order to gain insight into the atmospheric influence on the Southern Ocean circulation we have calculated the vertical movements in the upper layer as exerted by the surface wind stress.

Using surface winds when available and lowest level wind otherwise, we computed the wind stress for the four models. The vertical velocity at the bottom of the Ekman layer is related to the curl of the wind stress by the following equation:

$$\omega_{\mathrm{E}}(0) = -\mathrm{curl}\left(\frac{\tau}{\rho f}\right) \quad (1)$$

where $\omega_{\mathrm{E}}(0)$ is the vertical velocity at the bottom of the Ekman layer, τ the wind stress, ρ the ocean density and f the Coriolis parameter.

Therefore, in the Southern Hemisphere (where f is negative), a positive (negative) curl of the wind stress indicates zones of convergence (divergence) of the Ekman transport, and therefore downward (upward) motion in the ocean.

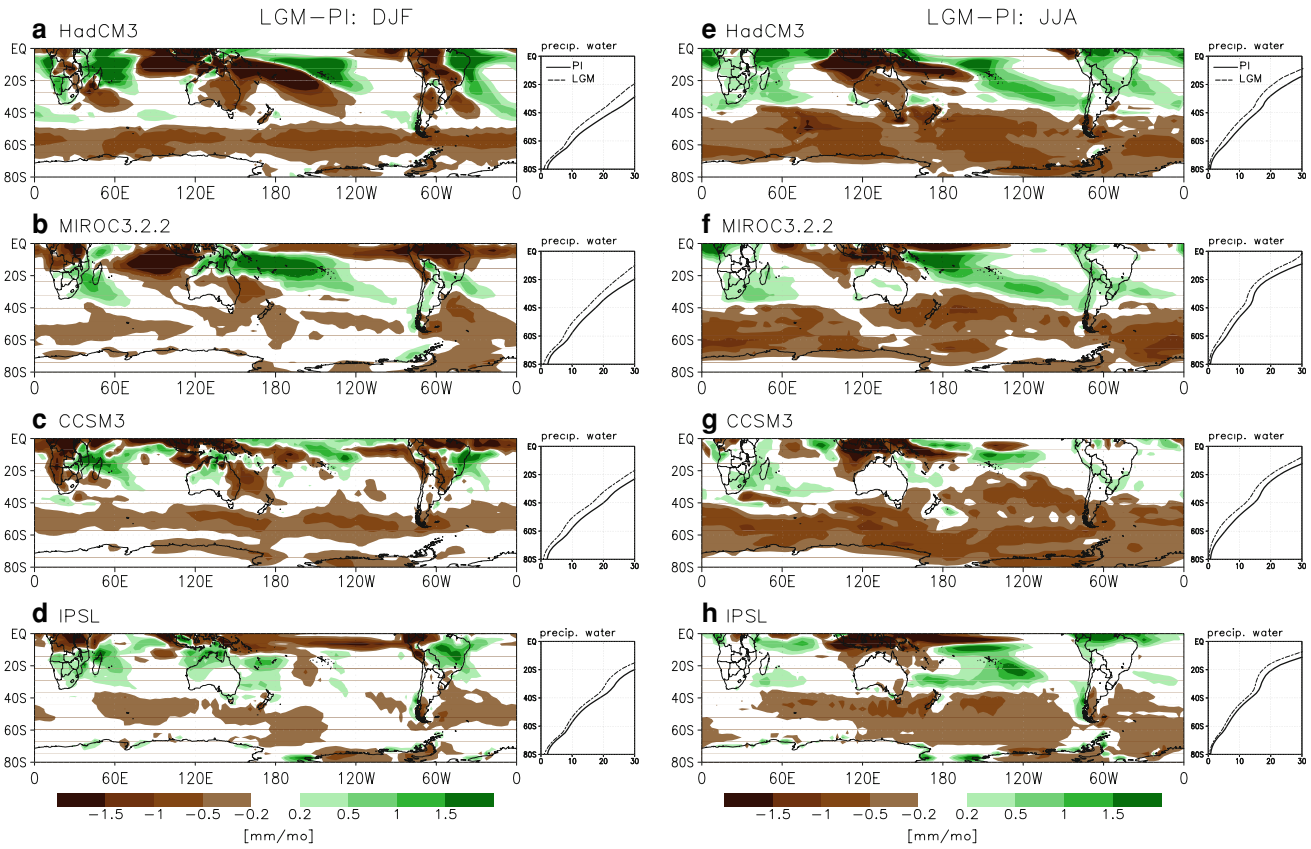

Fig. 14 Precipitation differences (LGM–PI) and zonal mean precipitable water profiles, for summer (*left panels*) and winter (*right panels*) for the four models

Inspection of the the zonal wind stress component and the wind stress curl, revealed a longitudinally homogeneous structure both in summer and winter. Considering this, we continued this analysis with the zonal average of these fields. Figure 15 shows in solid lines the zonal component of the wind stress and in dashed lines the curl of the wind stress, black lines corresponds to the PI simulation and blue lines to the LGM. The figure shows both in summer and winter a region around 45°–50°S with large positive wind stress and about 5 degrees south of the maximum wind stress a zone of large divergence (negative wind stress curl) and hence a region of upwelling.

Comparing the black (PI) and blue (LGM) lines, we see almost no changes in summer, except in HadCM3, that simulates an equatorward shift as well as a contraction of the divergence and zonal wind stress region. In winter HadCM3, MIRCOC3.2.2 and IPSL simulate a small decrease in the Ekman divergence and hence less upwelling in this region of the Southern Ocean, i.e. reduced overturning of the Southern Ocean deep waters. The exception is CCSM3, that simulates more divergence of the Ekman transport during the LGM compared to present day and therefore more upwelling. These results are coherent with the discussed changes in near surface circulation, and temperature and SLP gradients.

4 Summary and conclusions

We have presented paleoclimatic simulations for the Southern Hemisphere from four coupled AO GCMs for the Last Glacial Maximum climate. Our evaluation of the simulation of pre industrial conditions revealed that all models capture the important features of the Southern Hemisphere climate, although some significant biases became evident. HadCM3 provides a good simulation of the Southern Hemisphere atmospheric circulation: strength, position and seasonal evolution of both near surface and upper level winds. MIROC3.2.2, CCSM3 and IPSL have problems modelling the correct seasonal evolution of the jet-streams in the upper troposphere, failing to simulate the observed double-jet structure in winter. The biases in the winds are related to systematic errors in SLP and their meridional gradients. All models show significant biases in surface temperature, both in the atmosphere and at the sea surface. For the precipitation the models have some problems with the main convergence zones of the Southern Hemisphere.

The four models forced by the PMIP2-defined LGM boundary conditions simulate a colder climate to different degrees. All four models simulate smaller cooling in

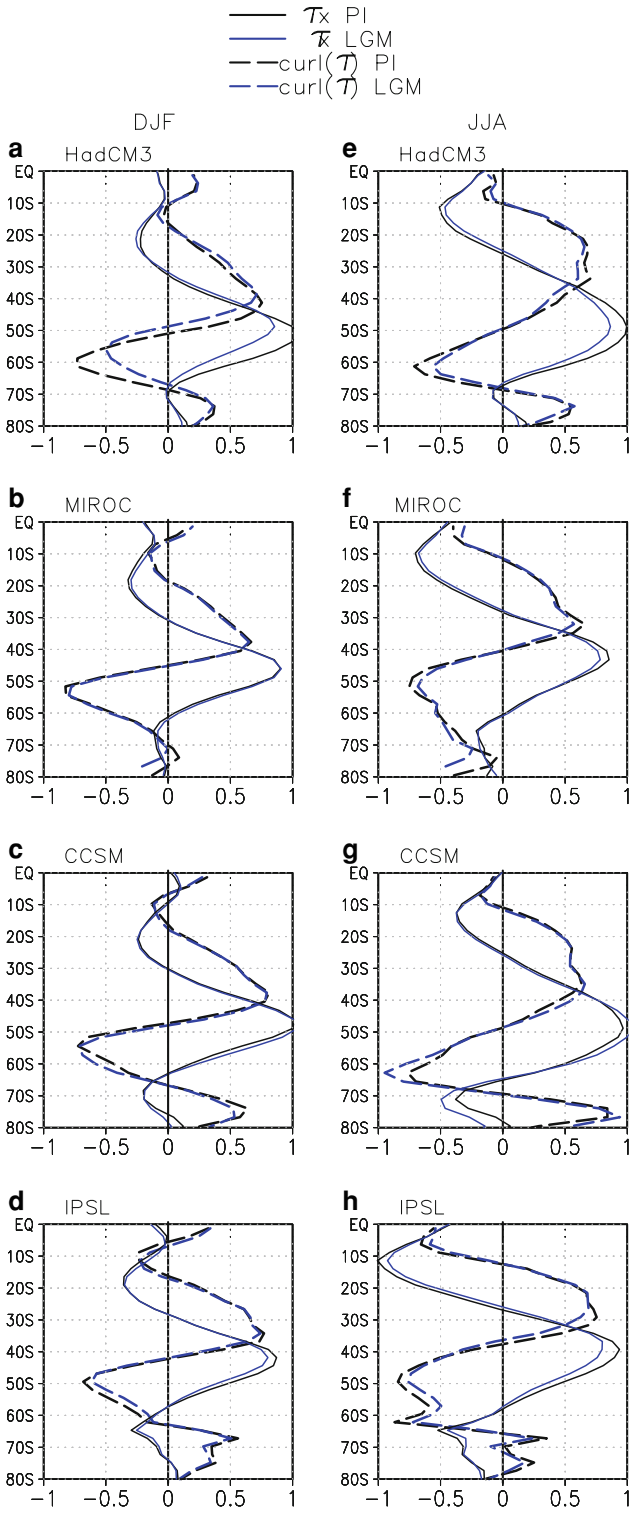

Fig. 15 Zonal mean profiles of curl of wind stress (*solid lines*) and zonal wind stress (*dashed lines*). *Black lines* PI simulation, *blue lines* LGM simulations

Australia than paleoclimatic estimates (ΔT = 2–5° vs. ΔT = 6–10°, Turney et al. 2006). Over southern South America and Antarctica the cooling is more in agreement with proxies (ΔT = 8–10° and ΔT = 10–15°, respectively, Moreno et al. 1997; Heusser et al. 1999; Stenni et al. 2001).

With respect to the atmospheric circulation, results differ among seasons. In summer changes are small with little common patterns. In winter some clearer patterns of change emerge. Additionally, changes are larger in the Pacific Ocean than in the other basins. Three out of the four models (HadCM3, MIROC3.2.2, and IPSL) simulate weaker winds in winter at 925 and 200 hPa, these are related to decreased SLP gradient and decreased mid-tropospheric temperature gradients, respectively. Therefore, although for the LGM the pole to equator surface temperature gradient increases, the gradient at mid-tropospheric levels actually decreases, with the consequence of a weaker atmospheric circulation. CCSM3 is the exception, apart from a weaker SPJ in winter, this model simulates a more vigorous atmospheric circulation during the LGM. This can be understood by the large temperature and sea-ice response to LGM forcings in the model.

Although none of the models simulate significant changes in the latitudinal position of the jet streams and the maximum wind speed regions, HadCM3, MIRCO3.2.2 and IPSL simulate a narrower STJ, apparently related to reduced midlatitude baroclinic zones in the LGM simulations relative to the present day; and weaker wind speeds at the near surface. As a result of these changes, at the near surface the region between 20° and 35°S shows stronger winds than PI in winter and weaker winds between 35° and 50°S. We observe diminished winds from 20° to 60°S at 200 hPa in summer and winter in these models.

Regarding the storm tracks, indicated by the cyclone density over a certain region, all models indicate increased storm activity in winter in midlatitudes (25°–45°S) and south of 60°S over the Pacific ocean. But, as with the atmospheric circulation, no significant shifts in the regions of maximum storm tracks are evident. Over the Pacific ocean there is a significant increase in storms during summer and winter. Although models simulate more storms at some longitudes south of about 60°S in the LGM, this increase is not accompanied by an increase in precipitation in the region. This is probably a consequence of lower precipitable water at these latitudes during the LGM.

The changes in precipitation patterns in all models indicate a general decrease south of 40°S. Agreement is found especially over the oceans, with some discrepancies over land. As a summary of the changes over the Pacific ocean, Fig. 16 shows the zonal mean profiles of winds, storm tracks and precipitation of the four models. From this summary figure there seems to be no direct link between the change in storm tracks and change in atmospheric winds. As discussed above, there are no large displacements in the position of zonal winds themselves where these cyclones are embedded in. Because storm tracks

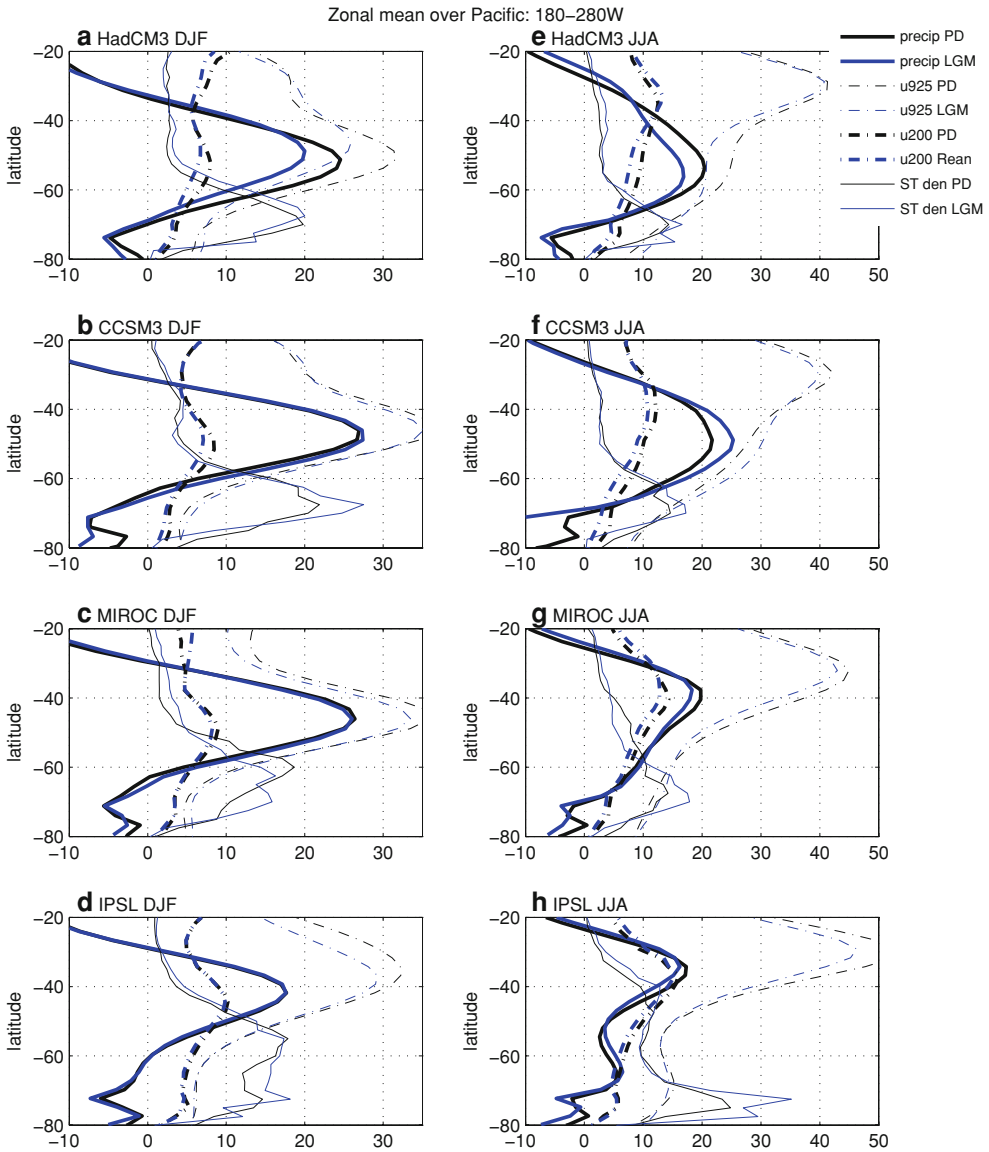

Fig. 16 Zonal mean profiles over the Pacific Ocean: 180–280°W of 925 and 200 hPa winds (m/s), storm track density and Precipitation (mm/mo) of all four models. *Black lines* PI simulation, *blue lines* LGM simulations

reflect the atmospheric baroclinicity they might also be influenced by other variables, such as changes in the SST gradients.

The relation between changes in the SST gradients and their influence on the Southern Hemisphere storm tracks is analysed and discussed in Inatsu and Hoskins (2004). They performed a number of experiments changing the SST gradients in the tropics as well as in the midlatitudes and evaluated their effect on the upper-level and low-level storm Track. They found that a reduction in the meridional SST gradient in the midlatitudes (south of 35°S) induces a decrease in the the low-level storm track in this region (measured as the meridional temperature gradient at 850 hPa in their case).

When comparing the SST gradients between LGM and PI, we find that the models simulate an important decrease of the SST gradient south of 50°, especially in winter. In summer only HadCM3 and CCSM3 show this feature. MIROC3.2.2 and IPSL simulate much smaller changes in the SST gradients, this is probably due to the smaller changes in sea-ice cover and is also reflected in small surface temperature changes over the oceans in these models (see Fig. 2). In winter there is an increase of the SST gradient between 40 and 45°S, coinciding with the region of increased storms.

Bengtsson et al. (2006) examined the causes of storm tracks changes in the Southern Hemisphere according ECHAM5 simulational for present day versus climate

change simulations (the IPCC SRES A1B scenario). They found systematic poleward shifts of the Southern Hemisphere storm tracks, and in the zone of maximum SST gradient. The results of Bengtsson et al. (2006) are further validated by Yin (2005), who reported on a consistent poleward shift of the Southern Hemisphere storm tracks by analysing climate change simulations (from the SRES A1B scenario) in 15 models. In that paper the storm tracks are represented by the vertically integrated 2–8 day Eddy Kinetic Energy. We note that these conclusions, based on "greenhouse" or "extreme interglacial" conditions have the opposite effect on the atmosphere-ocean interphase at mid- to high latitudes, than our findings on the PMIP2 simulations based on glacial boundary conditions.

The results reported in this paper, based on four coupled GCMs, do not find a definite "shift" in the westerly circulation, but suggest a general decrease in surface wind speeds in the Southern Ocean and sub-Antarctic sectors. This decline, in practise, could induce a similar effect as the hypothesised equatorward shift of the southern margin of the southern westerlies. We also found decreased upwelling over a longitudinal homogeneous region of the Southern Ocean, due to reduced near surface wind speeds. This change, coupled with a notable expansion in modelled sea-ice, lend support to the scenario proposed by Toggweiler et al. (2006) and Sigman and Boyle (2000) to account for oceanographic conditions and glacial/interglacial variations in atmospheric carbon dioxide. These GCM simulations might be sufficient to support Toggweiler's hypothesis, but a more complete analysis of the ocean circulation should be carried out.

We have analysed four models in this study, and this has shown us that despite the identical forcing applied to the four models we detect diverse, even opposite responses. The models also show regional heterogeneities, contributing to the view, only more recently acknowledged, of a less zonally symmetric Southern Hemisphere (e.g. general drying south of 40°S, but wetter NW Patagonia). In particular larger changes are found during winter and over the Pacific ocean.

We found that the cooling of the atmosphere during the LGM is not accompanied by an increase in tropospheric baroclinicity, as measured by the meridional temperature gradients. In fact, although at the surface the models simulate increased temperature gradients in winter (in summer changes are not significant), at higher levels, the midlatitude baroclinic zones are reduced, inducing a weakened atmospheric circulation, except at latitudes south of 70°S. There the temperature gradients are steeper at the surface as well as throughout the troposphere. Therefore, coming back to the questions enounced in the introduction, results of our analysis suggest that: (1) Three out of four models simulate a less baroclinic atmosphere and hence abated westerly circulation. (2) We do not see any significant shift in the westerly circulation during the LGM, however decreased wind speeds are found at the surface and the upper troposphere, with a narrower Subtropical Jet. (3) The LGM storm tracks did not exhibit either a significant latitudinal shifts. (4) Mayor circulation changes occur in winter and over the Pacific ocean.

Another interesting finding is that, despite regional heterogeneities and inter-model divergences, there seems to be a climate boundary between the mid- and high-latitudes of the Southern Hemisphere during the LGM. This discontinuity, which develops north and south of the zone of maximum wind speeds at 45–50°S is well expressed in several diagnostic features (maximum SLP gradient, SSTs, near-surface wind speeds, precipitation, cyclone density). We can only speculate that this transition might reflect the interface between regions dominated by an "Antarctic" versus a "rest of the world" palaeoclimate pattern during the LGM (Blunier and Brook 2001; Broeckner 1998; Denton et al. 1999; Moreno et al. 2001; Sugden et al. 2005).

Acknowledgments We acknowledge the international modelling groups for providing their data for analysis, the Laboratoire des Sciences du Climat et de l'Environnement (LSCE) for collecting and archiving the model data. The PMIP2/MOTIF Data Archive is supported by CEA, CNRS, the EU project MOTIF (EVK2-CT-2002-00153) and the Programme National d'Etude de la Dynamique du Climat (PNEDC). The analyses were performed using version mm-dd-yyyy of the database. More information is available on http://pmip2.lsce.ipsl.fr/ and http://motif.lsce.ipsl.fr. This investigation was supported by the FONDECYT grant # 1050416 and Institute of Ecology and Biodiversity, IEB. M. Rojas also thanks the ACT19 project. Disussion with Aldo Montecino on the ocean analysis and comments of two anonymous reviewers contributed greatly to the final version of the paper.

References

Alloway BV, Stewart RB, Neall VE, Vucetich CG (1992) Climate of the last glaciation in New Zealand, based on aerosolic quartz influx in an andesitic terrain. Quat Res 38:170–179

Bengtsson L, Hodges K, Roeckner E (2006) Storm tracks and climate change. J Clim 19:3518–3543

Blunier T, Brook EJ (2001) Timing of millennial-scale climate change in Antarctica and Greenland during the last glacial period. Science 291:109–112

Braconnot P, Otto-Bliesner B, Harrison S , Joussaume S, Peterschmitt J-Y, Abe-Ouchi A, Crucifix M, Driesschaert E, Fichefet Th, Hewitt CD, Kageyama M, Kitoh A, Laine A, Loutre M-F, Marti O, Merkel U, Ramstein G, Valdes P, Weber SL, Yu Y, Zhao Y (2007) Results of PMIP2 coupled simulations of the mid-Holocene and last glacial maximum—Part 1: experiments and large-scale features. Clim Past 3:261–277

Broecker WS (1998) Paleocean circulation during the last deglaciation: a bipolar seesaw? Paleoceanography 13:119–121

CLIMAP (1981) Seasonal reconstructions of the earth's surface at the last glacial maximum. Map Chart Series MC-36. Geological Society of America, Boulder, CO

Collins WD, Bitz CM, Blackmon ML, Bonan GB, Bretherton CS, Carton JA, Chang P, Doney SC, Hack JJ, Henderson TB, Kiehl JT, Large WG, McKenna DS, Santer BD, Smith RD (2006) The community climate system model Version 3 (CCSM3). J Clim 19:2122–2143

Denton GH, Lowell TV, Moreno PI, Andersen BG, Schlücher C (1999) Interhemispheric linkage of palaeoclimate during the last glaciation. Geogr Ann Ser A Phys Geogr 81A:107–153

Douglass DC, Singer BS, Kaplan MR, Ackert RP, Mickelson DM, Caffee MW (2005) Evidence of early Holocene glacial advances in southern South America from cosmogenic surface-exposure dating. Geology 33:237–240

Garreaud R (2007) Precipitation and circulation covariability in the extratropics. J Clim 20:4789–4797

Heusser CJ (1989) Southern westerlies during the last glacial maximum. Quat Res 31:423–425

Heusser CJ, Heusser LE, Lowell TV (1999) Paleoecology of the southern Chilean Lake District–Isla Grande de Chiloe during middle–late Llanquihue glaciation and deglaciation. Geogr Ann Ser A Phys Geogr 81:231–284

Hewitt CD, Stouffer RJ, Broccoli AJ, Mitchell JFB, Valdes PJ (2003) The effect of ocean dynamics in a coupled GCM simulation of the last glacial maximum. Clim Dyn 20:203–218. doi: 10.1007/s00382-002-0272-6

Imbrie J, Boyle EA, Clemens SC, Duffy A, Howard WR, Kukla G, Kutzbach J, Martinson DG, McIntyre A, Mix AC, Molfino B, Morley JJ, Peterson LC, Pisias NG, Prell WL, Raymo ME, Schackleton NJ, Toggweiler JR (1992) On the structure and origin of major glaciation cycles 1. Linear responses to Milankovitch forcing. Paleoceanography 7:701–738

Inatsu M, Hoskins BJ (2004) The zonal asymmetry of the Southern Hemisphere winter storm track. J Clim 17:4882–4892

Joussaume S, Taylor KE, Braconnot P, Mitchell JFB, Kutzbach JE, Harrison SP, Prentice IC, Broccoli AJ, Abe-Ouchi A, Bartlein PJ, Bonfils C, Dong B, Guiot J, Herterich K, Hewitt CD, Jolly D, Kim JW, Kislov A, Kitoh A, Loutre MF, Masson V, McAvaney B, McFarlane N, de Noblet N, Peltier WR, Peterschmitt JY, Pollard D, Rind D, Royer JF, Schlesinger ME, Syktus J, Thompson S, Valdes P, Vettoretti G, Webb RS, Wyputta U (1999) Monsoon changes for 6000 years ago: results of 18 simulations from the Palaeoclimate Modeling Intercomparison Project (PMIP). Geophys Res Lett 26:859–862

Kageyama M, Valdes P, Ramstein G, Hewitt C, Wyputta U (1999) Northern Hemisphere storm tracks in present day and Last Glacial Maximum climate simulations: a comparison of the European PMIP models. J Clim 12:742–760

Kalnay E, Coauthors (1996) The NCEP/NCAR 40-Year reanalysis project. Bull Am Meteor Soc 77:437–471

Kim SJ, Flato GM, Boer GJ (2003) A coupled climate simulation of the Last Glacial Maximum, Part2: approach to equilibrium. Clim Dyn 20:635–661

Kitoh A, Murakami S, Kiode H (2001) A simulation of the last glacial maximum with a coupled atmosphere–ocean GCM. Geophys Res Lett 28:2221–2224

Lamy F, Hebbeln D, Wefer G (1998) Late quaternary precessional cycles of terrigenous sediment input off the Norte Chico, Chile (27.5 degrees S) and palaeoclimatic implications. Palaeogeogr Palaeoclimatol Palaeoecol 140:233–244

Lamy F, Hebbeln D, Wefer G (1999) High-resolution marine record of climatic change in mid-latitude Chile during the last 28,000 years based on terrigenous sediment parameters. Quat Research 51:83–93

Levitus S (1994) NOAA Atlas NESDIS, World Ocean Atlas, U.S. Govt. Printing Office

Moreno PI (1997) Vegetation and climate change near Lago Llanquihue in the Chilean Lake District between 20,200 and 9500 14C yr B.P. J Quat Sci 12:434–441

Moreno PI, Leon A (2003) Abrupt vegetation changes during the last glacial to Holocene transition in mid-latitude South America. J Quat Sci 18:787–800

Moreno PI, Jacobson GL, Andersen B, Lowell TV, Denton GH (1999) Abrupt vegetation and climate changes during the last glacial maximum and the last Termination in the Chilean Lake District: A case study from Canal de la Puntilla (41°S). Geografiska Annaler Series A-Physical Geography 81A:285–311

Moreno PI, Jacobson GL, Lowell TV, Denton GH (2001) Interhemispheric climate links revealed from a late-glacial cool episode in southern Chile. Nature 409:804–808

Otto-Bliesner B, Brady E, Clauzet G, Thomas R, Levis S, Kothavala Z (2006) Last glacial maximum and Holocene climate in CCSM3. J Clim 19:2526–2544

Peltier WR (1994) Ice age paleotopography. Sci 265:195–201

Peltier WR (2004) Global glacial isostasy and the surface of the ice-age Earth: the ICE-5G (VM2) model and GRACE. Ann Rev Earth Planet Sci 32:111-149

Reynolds RW, Smith TM (1994) Improved global sea surface temperature analyses using optimum interpolation. J Clim 7:929-948

Schaefer JM, Denton GH, Barrell DJA, Ivy-Ochs S, Kubik PW, Andersen BG, Phillips FM, Lowell TV, Schluchter C (2006) Near-synchronous interhemispheric termination of the last glacial maximum in mid-latitudes. Science 312:1510–1513

Shin SI, Lui Z, Otto-Bliesner B, Brady EC, Kutzback JE, Harrison SP (2003) A simulation of the last glacial maximum climate using the NCAR-CCSM. Clim Dyn 20:127-151. doi:10.1007/s00382-002-0260-x

Shulmeister J, Goodwin I, Renwick J, Harle K, Armand L, McGlone MS, Cook E, Dodson J, Hesse PP, Mayewski P, Curran M (2004) The Southern Hemisphere westerlies in the Australasian sector over the last glacial cycle: a synthesis. Quat Int 118–119:23–53

Sigman DM, Boyle EA (2000) Glacial/interglacial variations in atmospheric carbon dioxide. Nature 407:859–865

Simmonds I, Keay K (2000) Mean Southern Hemisphere extratropical cyclone behaviour in the 40-year NCEP-NCAR reanalysis. J Clim 13:973–885

Simmonds I, Murray RJ (1999) Southern extratropical cyclone behaviour in ECMWF analysis during the FROST Special Observing Periods. Wea Forecasting 14:878–891

Simmonds I, Murray RJ, Leighton RM (1999) A refinement of cyclone tracking methods with data from FROST. Aust Meteor Antarctic Mag Special Issue, pp 35–49

Stenni B, Masson-Delmotte V, Johnson S, Jouzel J, Longinelli A, Monnin E, Rothlisberger R, Selmo E (2001) An oceanic cold reversal during the last deglaciation. Science 293:2074–2077

Sugden DE, Bentley MJ, Fogwill CJ, Hulton NRJ, Mcculloch RD, Purves RS (2005) Late-glacial glacier events in Southernmost South America: A blend of 'Northern' and 'Southern' Hemispheric climate signals? Geogr Anna Ser A Phys Geogr 87:273–288

Toggweiler JR, Russel J, Carson SR (2006) Midlatitude westerlies, atmospheric CO_2, and climate change during the ice ages. Paleooceonography 21:PA2005. doi:10.1029/2005PA001154

Turney CSM, Gaberle S, Fink D, Kershaw AP, Barbetti M, Barrows TT, Black M, Cohen TJ, Correge T, Hesse PP, Hua Q, Johnston R, Morgan V, Moss P, Nanson G, Van Ommen T, Rule S, Williams NJ, Zhao J-X, D'Costa D, Feng Y-X, Gagan M, Mooney S, Xia Q (2006) Integration of ice-core, marine and terrestrial records for the Australian last glacial maximum and termination: a contribution from the OZINTIMATE group. J Quat Sci 21(7):751–761

Valdes PJ (2000) South American paleoclimate model simulations: how reliable are the models? J Quat Sci 15:357–368

Valero-Garcés BL, Jenny B, Rondanelli M, Delgado-Huertas A, Burns SJ, Veit H, Moreno A (2005) Palaeohydrology of Laguna de Tagua Tagua (34° 30'S) and moisture fluctuations in Central Chile for the last 46 000 yr. J Quat Sci 20:625–641

Williams GP, Bryan K (2006) Ice age winds: an aquaplanet model. J Clim 19:1706–1715

Williams PW, Kingb DNT, Zhaoc J-X, Collerson KD (2005) Late Pleistocene to Holocene composite speleothem 18O and 13C chronologies from South Island, New Zealand-did a global Younger Dryas really exist? Earth Planet Sci Lett 230:301–317

Wyrwoll K-H, Dong B, Valdes P (2000) On the position of southern westerlies at the last glacial maximum: an outline of AGCM simulation results and evaluation of their implications. Quat Sci Rev 19:881–898

Xie P, Arkin PA (1996) Analyses of global monthly precipitation using gauge observations, satellite estimates, and numerical model predictions. J Clim 9:840–858

Yin JH (2005) A consistent poleward shift of the storm tracks in simulations of 21st century climate. Geophys Res Lett 32:L18701. doi:10.1029/2005GL023684